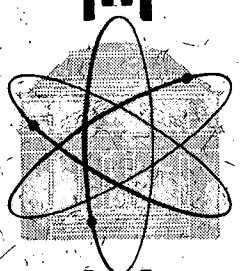

Research Laboratories for the Engineering Sciences

University of Virginia

Charlottesville

Report No. EME-4029-112-71U

November 1971

A FORCE BALANCE SYSTEM FOR THE MEASUREMENT OF SKIN FRICTION DRAG FORCE

FINAL REPORT FOR
NATIONAL AERONAUTICS AND SPACE ADMINISTRATION
GRANT NO. NGR 47-005-026

Submitted by:
Dr. J. W. Moore
Professor of Mechanical Engineering

Dr. E. S. McVey
Professor of Electrical Engineering

Division of Electrical Engineering
and
Division of Mechanical Engineering
RESEARCH LABORATORIES FOR THE ENGINEERING SCIENCES
SCHOOL OF ENGINEERING AND APPLIED SCIENCE
UNIVERSITY OF VIRGINIA
CHARLOTTESVILLE, VIRGINIA

Report No. EME-4029-112-71U
November 1971

Copy No. 5

TABLE OF CONTENTS

LIST OF FIGURES

FOREWORD

This is the final technical report for research on force balance instrumentation to measure the skin friction of hypersonic vehicles at extreme temperatures, high altitudes and in a vibration field, except for a minor effort on certain of the mechanical considerations. This report serves as a status report too because current research effort is reported.

Because the work has been so comprehensive only the most recent work is contained here. The other final detailed design and experimental data are presented in reports: EME-4029-109-69U, September 1969; EME-4029-110-70U, January 1970; EME-4029-111-70U, April 1970. They contain the great majority of the design type information. This report is intended to give only a rough overall summary and operating instructions for the equipment which was delivered to NASA on August 2, 1971.

During the course of the skin friction system work six students earned masters degrees and one earned a Ph.D. Five papers have been published or are in the final stages of publication on the research.

SECTION I

INTRODUCTION

Skin-friction drag occurs on the surface of a body due to shear stresses in adjacent layers of fluid moving relative to the body. At very high speeds, the skin-friction force becomes an appreciable factor in the total drag acting on flying-objects. As a result, the skin-friction drag is one of the limiting factors in speed attainment in atmospheric flight. Skin-friction drag not only consumes a large amount of vehicle power, but, equally important, it causes all exposed surfaces to heat up. It is, therefore, evident that an effective method for determining the magnitude of skin-friction force is of prime importance to the present-day designer of high-speed aircraft.

Much of the previous work deals with the attempt to discover the basic theoretical relation between skin-friction drag and factors such as: Reynolds Number, Mach Number, surface condition and heat transfer [1]. But it is apparent that a need exists for experimental skin-friction data to correlate with the results of theoretical predictions, thereby substantiating the analytical methods used in the determination of skin-friction.

Wind tunnels have long been an important tool for the experimental investigation of aerodynamic properties. The development of a free-flight skin-friction meter is essential because the free-flight Reynolds Number and stagnation temperature at high Mach Numbers are extremely difficult to simulate in wind tunnels and other testing devices.

Research work dealing with the development of a system for the direct measurement of skin-friction drag has been conducted as a joint effort between the Electrical and Mechanical Engineering Departments of the University of Virginia. The primary goal has been to develop a high-temperature skin-friction meter to aid in making thrust measurements of an experimental hypersonic ramjet. It was proposed to mount the ramjet below the X-15A-2 experimental aircraft and test it at altitudes up to 123,000 feet and at speeds up to Mach 8 [2]. The flight test program was dropped before completion of the system but the meter will be useful

for wind tunnel experimentation at high temperatures and is presently being installed in a test set-up. Although exact specifications were not available, development of the skin-friction meter was guided by the following specifications [2] which are believed to be adequate:

1) Force measurement range: The meter is to be capable of measuring a force in the range of 0.7 to 7 millipounds.
2) The meter must withstand sustained ambient temperatures of 2000°F.
3) Vibration: The meter is to be capable of operating in environmental levels of 0.06 inch double amplitude at 10-65 cps and 10 g vibration from 55 to 2000 cps.
4) Acceleration: The maximum translational acceleration attained in the direction of flight is 3.5 g.
5) Space requirements: The limiting dimension is the height (distance from skin to jet nozzle) which is 2 inches. The other two dimensions may be somewhat larger.
6) The maximum deflection of the target must not exceed 0.0005 inch. The target is a small area of the aircraft skin which is free to move a small amount when acted upon by a friction-drag force.

A good detailed discussion of the method for the early direct measurement of skin-friction force is given by Weiler [1]. Basically most of the skin-friction meters employed the so-called "floating element" technique. This method involves suspending a portion of the skin exposed to the air stream on a flexure (or other low friction pivot) so that it is free to move. If the flexure spring constant is known, a readout of the flexure position can be used for force determination. The schematic diagram shown in Fig. 1 is a general model of the stationary wind tunnel skin-friction meter. Two parallel flexures serve as the supporting mechanism. Due to the special characteristic of these two parallel flexures, for small displacements, the small floating disc will move in the x-axis only. The linear variable differential transformer (LVDT) senses the deflection and gives a voltage output.

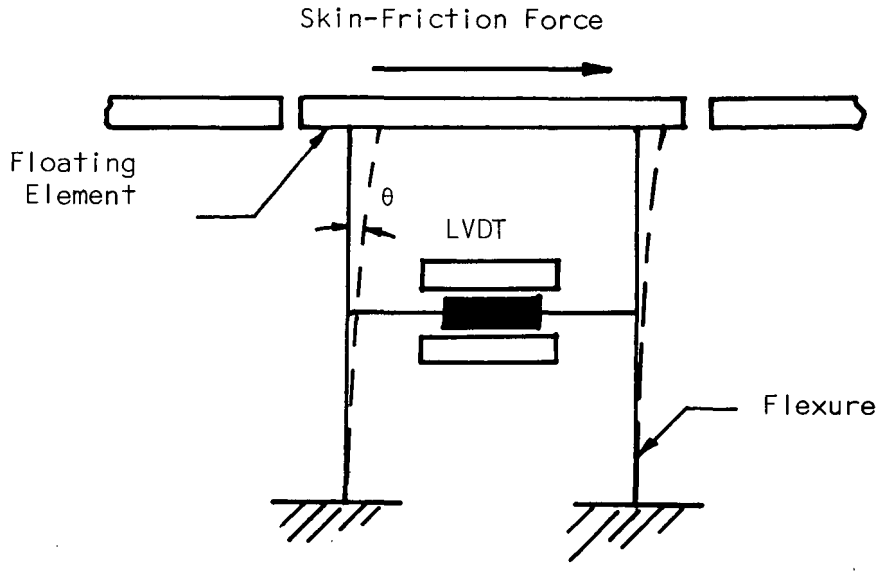

Figure 1. Schematic Diagram of An Open Loop System for Measuring Skin Friction

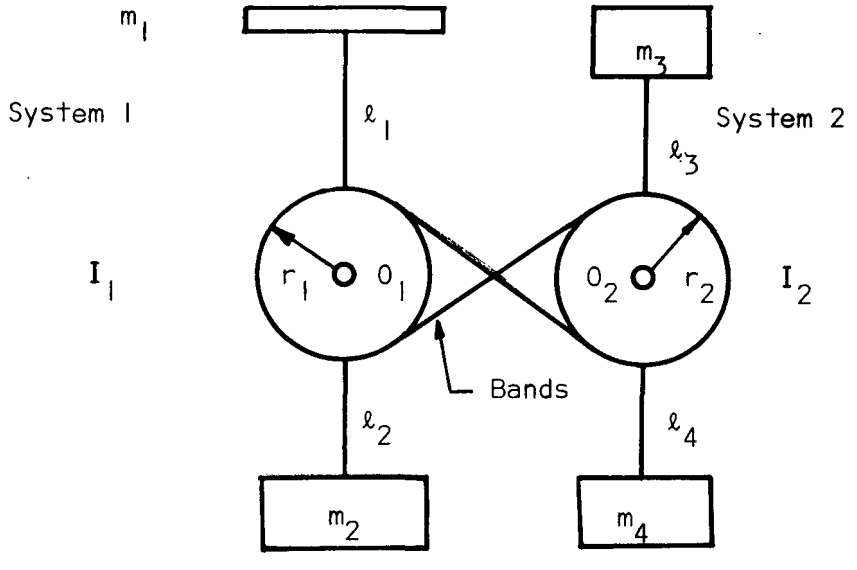

Figure 2. Schematic Diagram of System Configuration for Acceleration Insensitive Skin-Friction Meter

The schematic diagram in Fig. 2 shows a technique by Weiler [1] and Ashby [3] for counterbalancing a skin-friction meter and making the meter insensitive to accelerations and vibrations. The mass m_1 represents the floating element. The counterweights m_2, m_3, and m_4 are the design masses. System 1 is pivoted at O_1 and system 2 is pivoted at O_2. The lengths ℓ_1, ℓ_2, ℓ_3, and ℓ_4 are design values. The moment of inertia of system 1 about O_1 is I_1 and I_2 is the moment of inertia of system 2 about O_2. Systems 1 and 2 are coupled together by crossed thin metal bands wrapped around cylindrical surfaces fastened to each one of the two arms to which the counterweights are fastened. In Ashby's thesis [3] the conclusion is made that when

$$m_1\ell_1 = m_2\ell_2,$$

$$m_3\ell_3 = m_4\ell_4,$$

and

$$I_2 = \left(\frac{r_2}{r_1}\right)^2 I_1,$$

then the total system will be insensitive to both linear and angular accelerations.

One of the first operational systems of this type was used in the Aerobe-Hi missile [4]. A counter-balanced flexure system (as shown in Fig. 3) was used to support the target (floating element) and a linear variable differential transformer (LVDT) was used to convert flexure displacement into an electrical readout signal. This system is satisfactory for constant temperature environments. Temperature change causes changes in the flexure spring constant, LVDT constant and zero position. To overcome these difficulties a closed loop system can be used as indicated in Fig. 4.

A closed loop system generally the same as the system of Fig. 3 but without the counterbalancing system of Fig. 2 was developed by

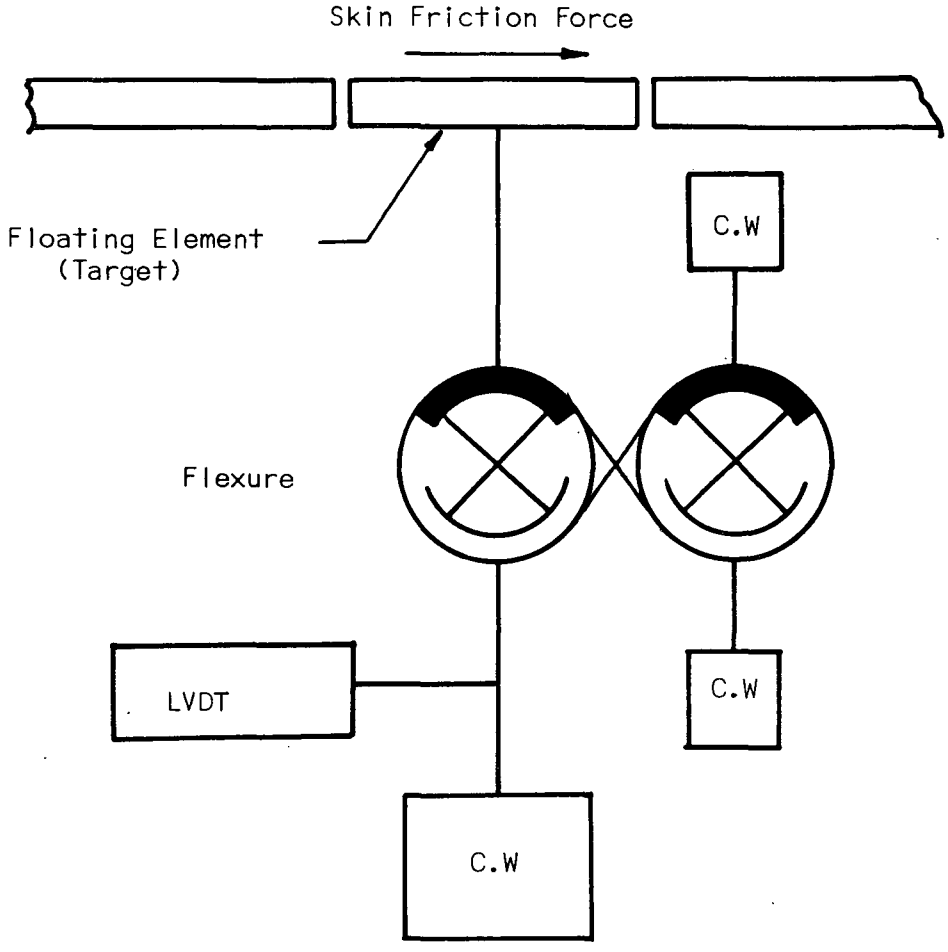

Figure 3. Schematic Diagram of An Acceleration Insensitive Open Loop Skin-Friction Meter

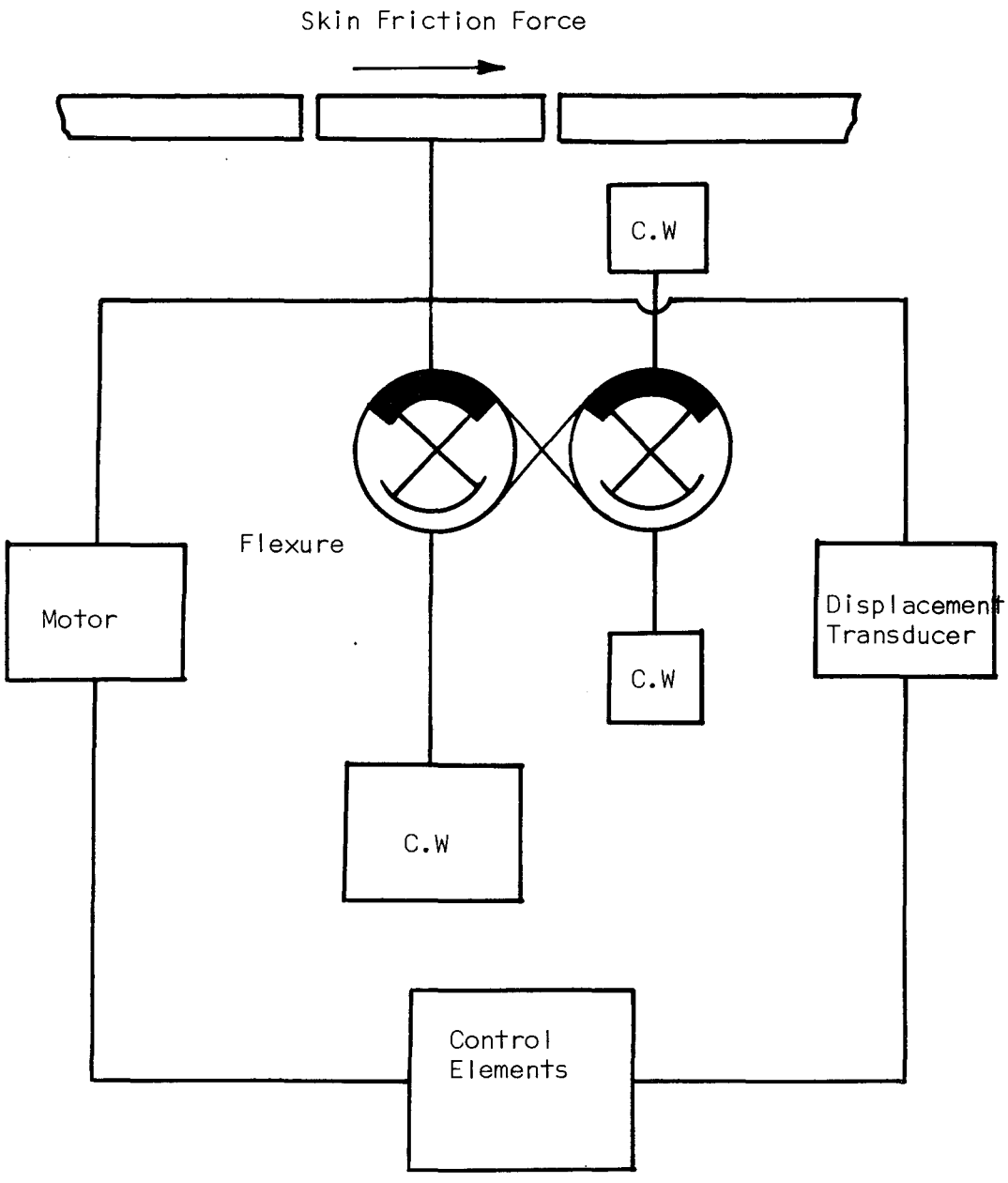

Figure 4. Schematic Diagram of a Closed Loop System for Measuring Skin Friction

Kistler [5]. A cooling jacket surrounds the Kistler instrument and makes operation possible from room temperature to 1000°F.

The ideal solution from a reliability and operational point of view is to design a counterbalancing system so that it is capable of operating continuously in the high temperature environment. Our previous work in the area of force measurement and engineering judgement indicated that a closed loop floating element method of measurement was the logical approach for the development of a high temperature skin-friction meter.

Early in the work it was decided that operations should be closed loop because the spring constant of all available flexure materials vary over a relatively large range when subjected to required temperature changes. This creates the need for a motor and associated servo control circuitry, but does make flexure constant variations negligible. The diagram of a general system is shown in Fig. 4 which is typical of all the closed loop systems. For electrical systems, the differential equation is

$$dF_x + \ell F_m - K_f\theta = J\ddot{\theta} \qquad (1)$$

where

F_x is skin friction drag force
K_f is the flexure constant
J is the rotational inertia of all moving parts
d is the distance from the target to the flexure
ℓ is the distance from the servo motor to the flexure

This equation is based on operation as follows: when a skin friction force, F_x, is present the flexure is displaced; the displacement is sensed by the transducer which has an output voltage proportional to displacement; the sensor output is amplified and used to drive the motor which produces a force in opposition to the skin friction force; motor armature current is proportional to motor force and is the system output measurement.

It is easy to show that the steady state armature current is

$$i_a(\text{steady state}) = -\frac{F_m}{K_m}\frac{d}{\ell} \tag{2}$$

by taking the Laplace transform of Eq. (1) and using the final value theorem for a step of force F_x. The motor constant relating i_a and F_x is K_m. The only assumption required is that $\ell^2 K_m K_s K_a >> R_a K_f$. This can be satisfied because the loop gain constant K_s is under the designers control. Other constants are R_a, the motor armature resistance, and K_a, the motor back emf constant. The complete dynamic equation is [4]

$$\frac{i_a(s)}{F_x(s)} = \frac{-d\ell K_v \; s + \left[\frac{K_s K_a}{K_v}\right]}{JR_a\left(s^2 + \frac{\ell K_m K_v}{JR_a}\, s + \frac{\ell^2 K_m K_a K_s + R_a K_f}{JR_a}\right)} \tag{3}$$

This information is typical of all three systems which are presented. Of course, the parameters are not the same for the different systems. The first system described is an electrical system which contains cobalt magnetic material. Next, an air-core type electrical system is presented and then the pneumatic system is presented. The last section briefly describes approaches and results of support systems including tests to 750°F of the model being installed in the NASA laboratory.

SECTION II

ELECTRICAL SYSTEM DEVELOPMENT

The use of electrical components for the measurement of force or torque in the range required for the measurement of skin friction is well established and offers very attractive advantages. However, there are no known motors or position sensors available nor, apparently, any literature describing even the problems of developing suitable components because of the required 2000°F operating temperature. It is necessary that the motor and sensor work in the 2000°F environment, but it is out of the question to consider operating the associated electronic instrumentation at 2000°F. Fortunately, in this application and many other applications for which the system components may be used, it is possible to operate the electronic package at ordinary temperatures. In the final design, six leads connect the motor-sensor assembly to the electronic package. The currents, voltages, and frequencies are all in a range convenient for such operation; and, since the motor works from current sources the extra lead resistance presents no problem. The sensor uses a relatively high impedance circuit so that lead resistance is unimportant, too. The sensor frequency, 5 KHz is high enough that filtering pick-up presents no problems.

Due to the advantages (e.g., size) afforded by the use of ferromagnetic material in motors, conventional motor design should be used wherever possible even if the permeability of the material is relatively low. However, there is no known ferro-magnetic material with a Curie temperature above 2050°F (cobalt), which is too close to the 2000°F temperature specification to be practical when the motor temperature rise is considered.

A. Cobalt Electrical System

Capacitor type motors working with electric fields were rejected when calculations indicated that relatively high voltages would be required. The voltages would present very difficult practical problems at high altitudes and temperatures.

Enough work was done [6] on a Cobalt Electric System capable of operation to approximately 1750°F to state that the idea is feasible. A schematic diagram of the motor is shown in Fig. 5. The armature consists of two E sections which work in a differential arrangement, i.e., the current increases in one field winding and decreases an equal amount in the other one. The rotor is a simple rectangular or I section. An identical structure is used for the position sensor as can be seen in the top view of the assembly in Fig. 5. It is possible to use both sets of coils to produce torque and also act as position sensors by superimposing a 20 KHz carrier frequency on the motor signal. This approach is recommended to reduce size and weight and to give symmetry for cancellation of thermal effects. Cantilever pivots are used to support the armature at the top and bottom so that it can rotate and change the displacements x_1 and x_2 shown in Fig. 5. Each coil contained 12 turns of #22 B & S 80-20 nichrome wire with Hi-Temp Wire Company woven quartz insulation. The rotor length is 1.375 inches, width is 0.500 inches and thickness is 0.250 inches. The E sections have corresponding dimensions and a window depth of 0.250 inches. The force generated by the motor can be derived from basic principles as

$$F = \frac{4\mu_o AN^2}{\sqrt{2}} \left[\frac{I_o \Delta I}{(\frac{\ell}{\mu_r} + x)^2} \right] \tag{4}$$

where

F = force

$x = x_1 + x_2$ = total air gap

I_o = quiescent current

ΔI = differential current

N = number of turns per coil

A = cross-sectional area of the magnetic material

μ_r = permeability of the magnetic material

μ_o = permeability of free space

ℓ = mean length of flux path in magnetic material (see Fig. 5)

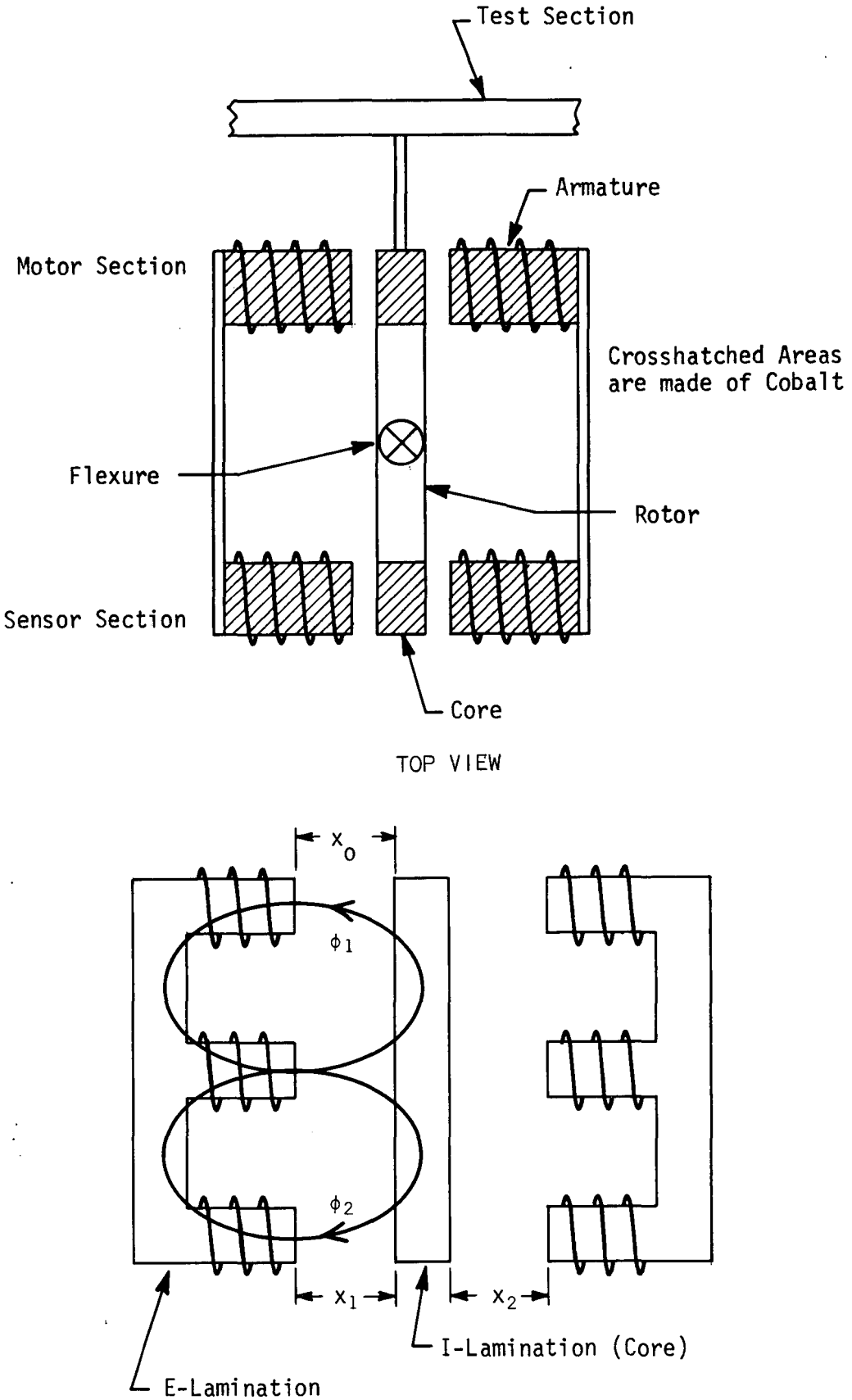

Figure 5 Schematic of Cobalt Motor-Sensor

Note that the force is a linear function of the differential current and an inverse square function of the air gap length. These factors are born out by the data of Fig. 6. Also note that the ratio of the flux path length to the core material permeability must be small compared to the air gap length if the force is to be independent of temperature as μ_r changes. For a 1.9 inch flux path and an air gap of 0.025 inches, a relative permeability of only 380 is required for a ten to one ratio of the two terms. This yields an acceptable error due to permeability change with temperature.

The force data of Fig. 6A extends into the third quadrant as an odd function. Sensor data are shown in Fig. 6B. Twelve turn coils were used for these data. Close loop operation [6] of the system demonstrated the feasibility of building a skin friction meter with cobalt magnetic material. The data were in accordance with the open loop motor data presented in Fig. 6. High temperature data were not taken but calculations on thermal effects lends further credence to the feasibility. Work was not carried thorugh to completion because of the superior high temperature capability of the air-core electrical and pneumatic systems.

B. Air-Core Electrical System

The air-core electrical system work was carried to the prototype stage in preference to the cobalt system because its theoretical temperature limit depends only on the wire, flexure, and ceramic coil-form material. Platinum coated molybdenum wire with quartz fiber insulation was found to be the most suitable wire material. The flexure bearings for the rotor are made of RA 330 stainless steel and the coil forms are made of hydrous aluminum silicate (lava). It was found that the platinum would migrate into the molybdenum at high temperatures and leave small voids on the surface of the wire where the molybdenum could be oxidized, so ceramic encapsulation of the coils was found to be desirable. Nichrome lead wire was used because of its good performance at high temperatures. Nichrome wire would be a good candidate for the coils too if production quantities of the systems were to be made. Quantity production would allow solution of the winding problems.

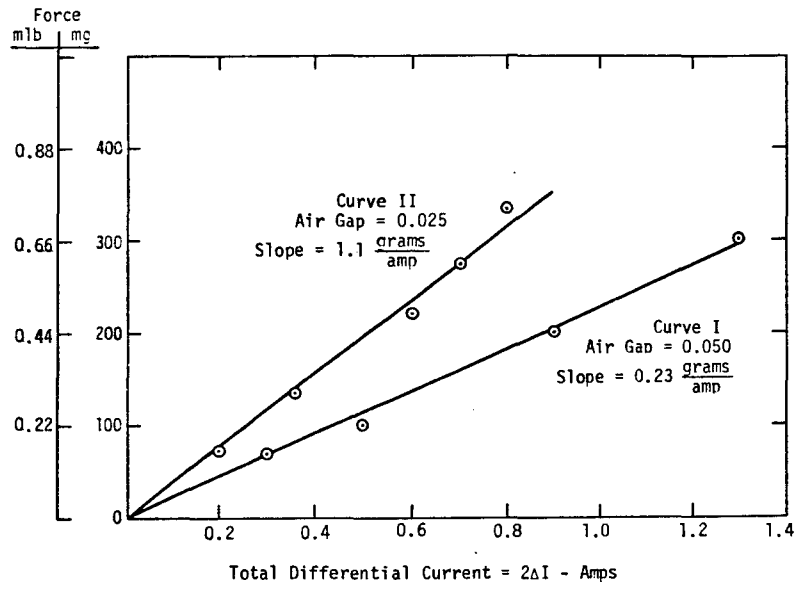

Figure 6A Cobalt Motor-Sensor Force Curves for Two E Sections and Two Amperes Quiescent Current

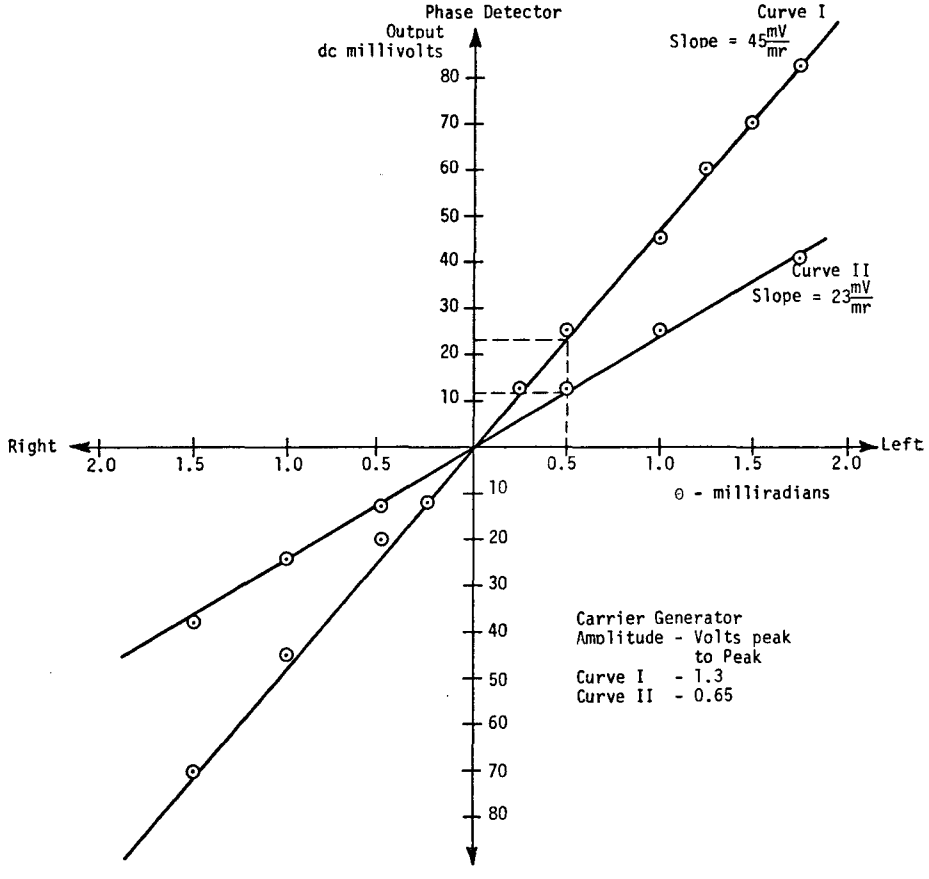

Figure 6B Cobalt Motor-Sensor Transfer Characteristics

A schematic of the motor-sensor assembly is shown in Fig. 7. Note that the rotor must be energized in this system, unlike the cobalt system. The flexures are used to conduct the armature current. This removes the possibility of tare forces that wires would introduce, but it does cause I^2R heating of the flexures. The rectangular construction was used because it was found that when the length, radius, and thickness are constrained the cross sectional shape enters into power minimization and that the coil length should be maximized for minimum power consumption (which affects self heating). Table I summarizes the design results of the motor-sensor assembley.

The theoretical torque was calculated [7] and agreed with the experimental value to within 5%. Closed loop data were taken on a motor-sensor assembly as shown in Fig. 8. The system operated satisfactorily to the 1300-1400°F range. A rough recording of temperature would allow calibration of data to better than 3%. However, the system failed above 1400°F. Air bubbles trapped during the coil encapsulation caused the ceramic to crack and allowed oxidation of the wire. However, it is not certain that the change in wire resistance caused the excessive null shift as indicated in Fig. 8. Thermal relief or expansion may have caused the problem. Note that motor linearity is not affected.

Unfortunately, the second motor-sensor assembly built has a thermally induced null shift problem and time has not permitted this problem to be corrected. The second unit is being installed in a test facility at NASA, Langley, Virginia. The test time is expected to be small compared to the heating time of the assembly, so satisfactory operation is anticipated in high temperature environments.

Feasibility of steady state system operation to 2000°F is believed to be established even though satisfactory steady-state data have not been obtained beyond 1400°F. Certainly, an instrument has been built and tested which will work for short periods of time in a 2000°F environment and for extended periods at lower temperatures.

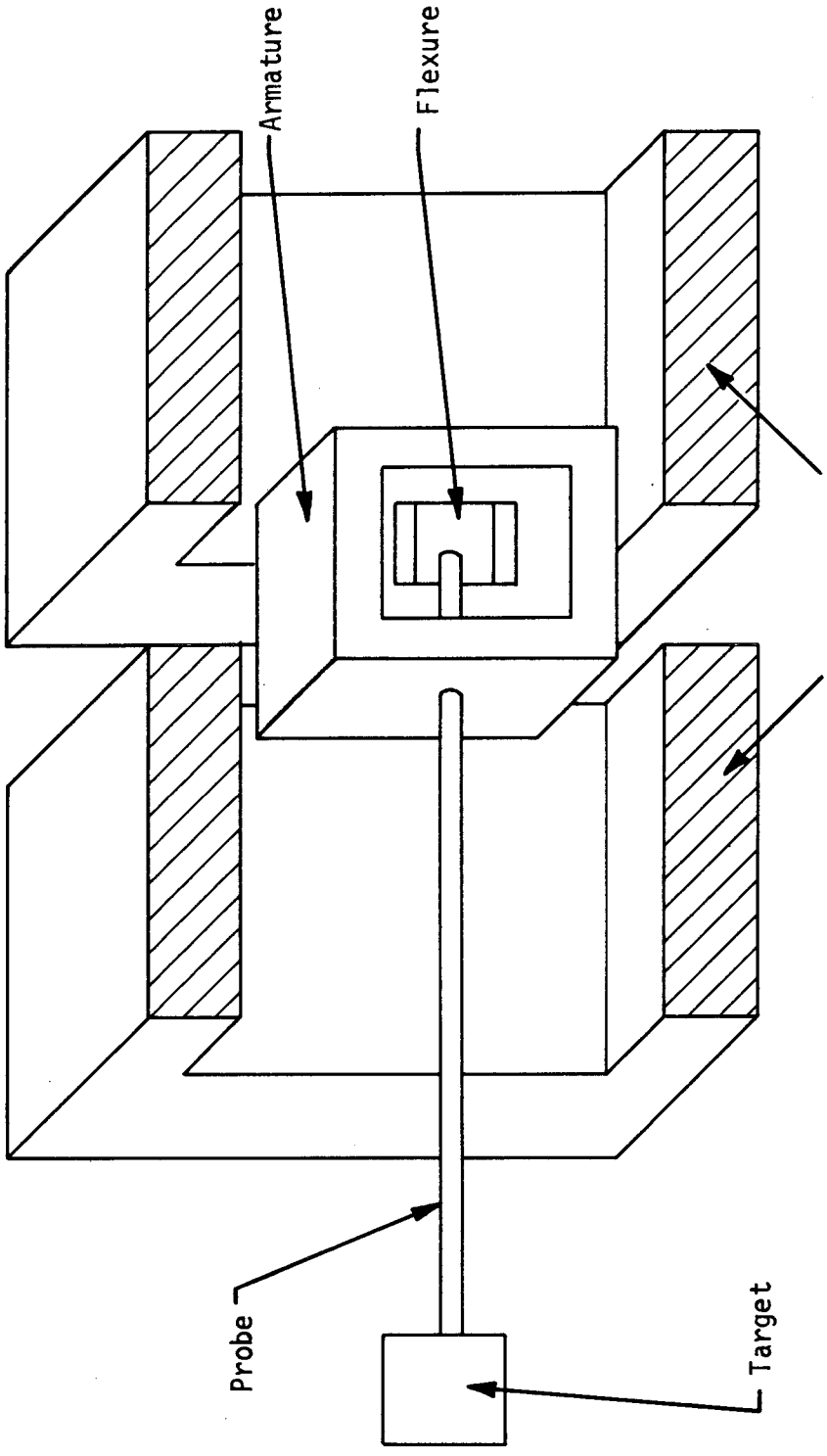

Figure 7 Air-Core Motor-Sensor Assembly

TABLE I

MOTOR PARAMETERS

	SYMBOL	DIMENSION
FIELD COILS		
Inside radius, inches	R	1.06
Overall length, inches	L	2.06
Winding thickness, inches	r_w	0.36
Gap Width, inch	G	0.40
Wire size, inch	d_w	0.032
No. turns per layer		11
Total No. turns/coil	N	55
Constant current, amps	I	3.5
Max power dissipation/coil	P	84
Temperature rise (15 min.)		480°F
ARMATURE COIL WEIGHT		
Inside radius, inch	R	0.59
Width, inches	C	1.68
Winding thickness, inch	r_w	0.21
Wire size	d_w	0.032
No. turns per layer		14
Total no. turns	N	42
Max power dissipation, watts	P	41
Temperature rise (15 min.)		230°F
Weight, lbs		0.262

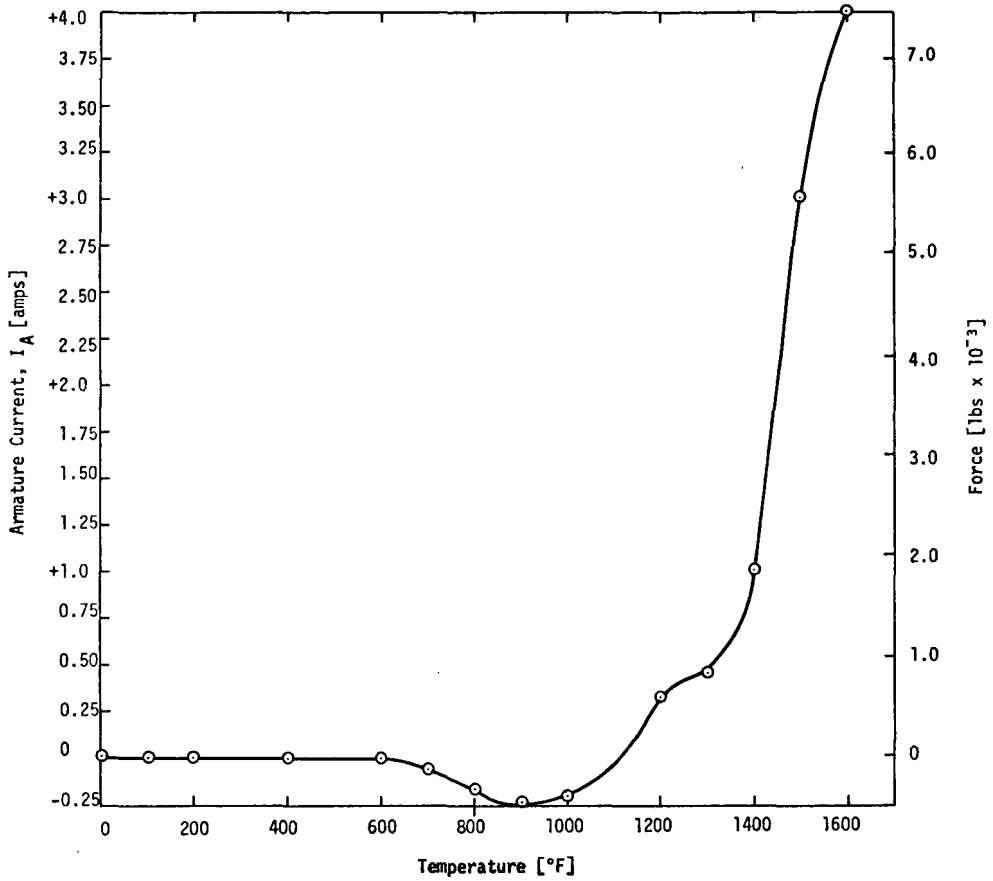

Figure 8A System Closed Loop Null

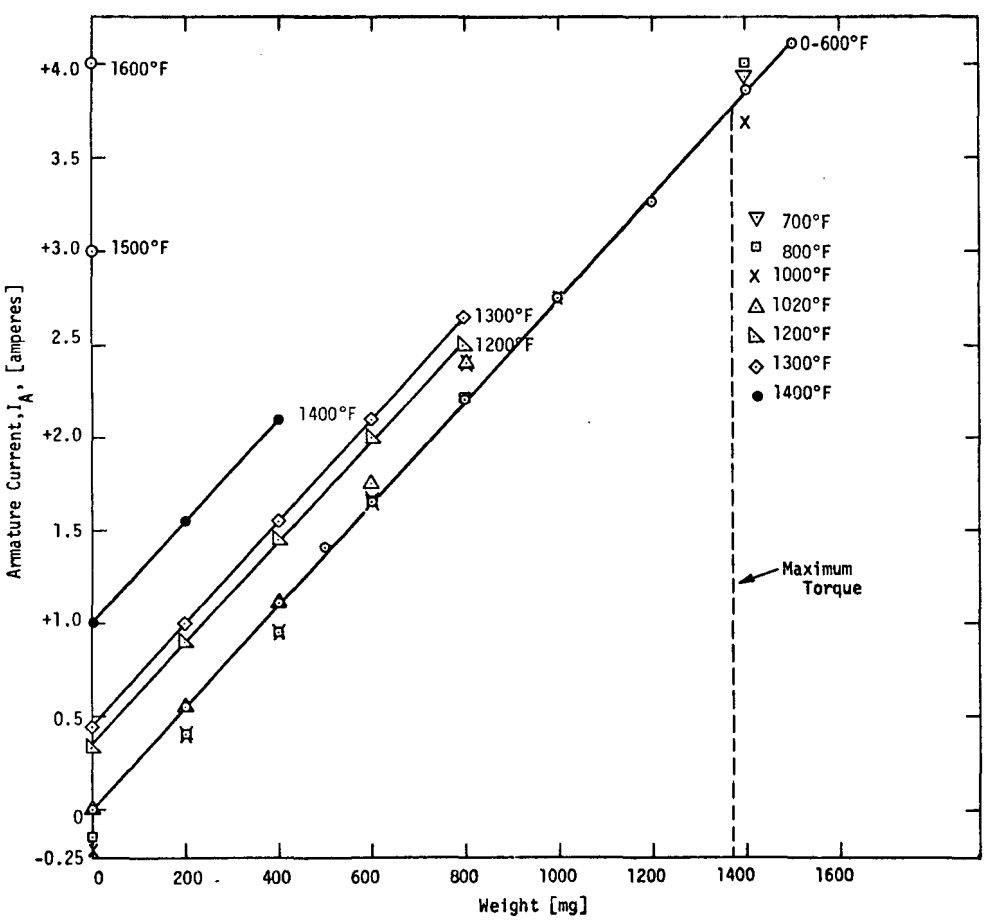

Figure 8B System Force Calibration

SECTION III

PNEUMATIC SYSTEM SENSING

The need for closed loop control as a means of sensing the target movement due to skin friction drag force has already been noted. The requirements for operation at very high temperature and that the target travel be very limited suggest that some form of pneumatic control might be appropriate. Such a system has been designed, its components individually tested, and a complete breadboard system successfully tested to 2000°F [8].

The basic part of the system is a pneumatic flapper valve supported in the same manner as the armature of the electrical system. Figure 9 shows a schematic diagram of the system and Fig. 10 shows a block diagram which is based on the differential equations of the system. The closed loop transfer function is:

$$\frac{C(s)}{T(s)} = \frac{G_1\{2\left.\frac{\partial Q}{\partial \theta}\right|_o G_5 + G_4 + (G_3 + \left.\frac{\partial Q}{\partial p}\right|_o G_5)G_2\}}{1 + G_1\{2\left.\frac{\partial Q}{\partial \theta}\right|_o G_5 + G_4 + G_3 + \left.\frac{\partial Q}{\partial p}\right|_o G_5)G_2\}} \qquad (5)$$

The individual block transfer functions were determined and verified experimentally for the component parts. With simplification, determination of the partials, the retention of only dominant terms, Eq. 5 can be represented by:

$$\frac{C}{T}(s) = \frac{172(s + 8600)}{(s + 45)(s^2 + 130s + 38600)} \qquad (6)$$

This transfer function is for motion of the flapper-target caused by the skin friction drag. The actual signal used to read-out the value of the drag is the ΔP across the flapper valve nozzles or across the air motors.

The initial approach to this system involved the use of the flapper valve as a position sensor, of beam deflection fluid amplifiers for gain and compensation, and of pressure motors to move the flapper towards null. Two major departures from this plan were made. One of these eliminated the need for compensation when it was discovered that the transmission

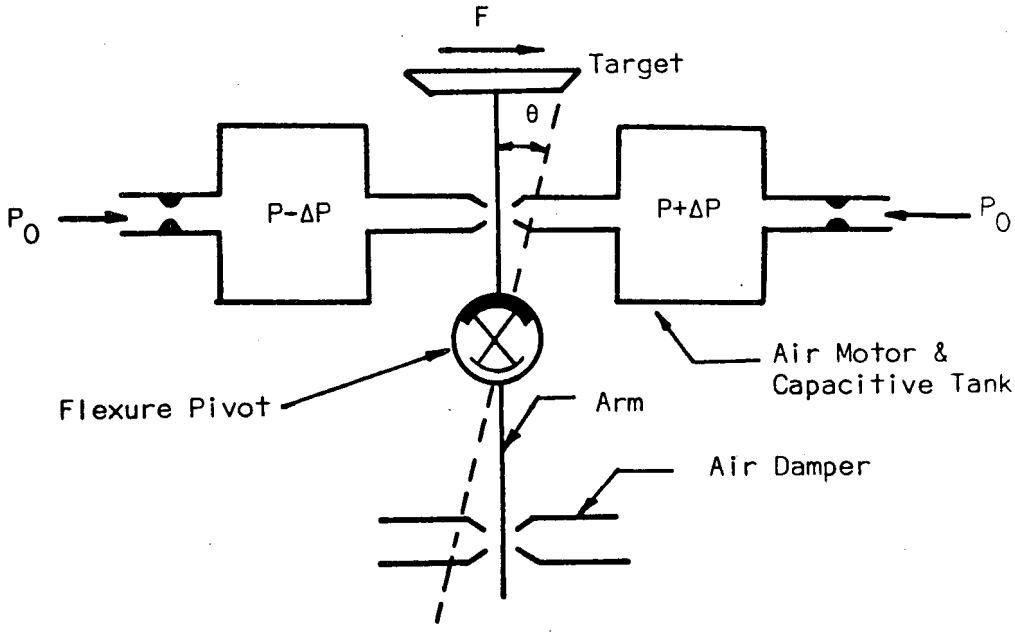

Figure 9 Schematic Diagram of a Pneumatically Controlled Skin-Friction Meter

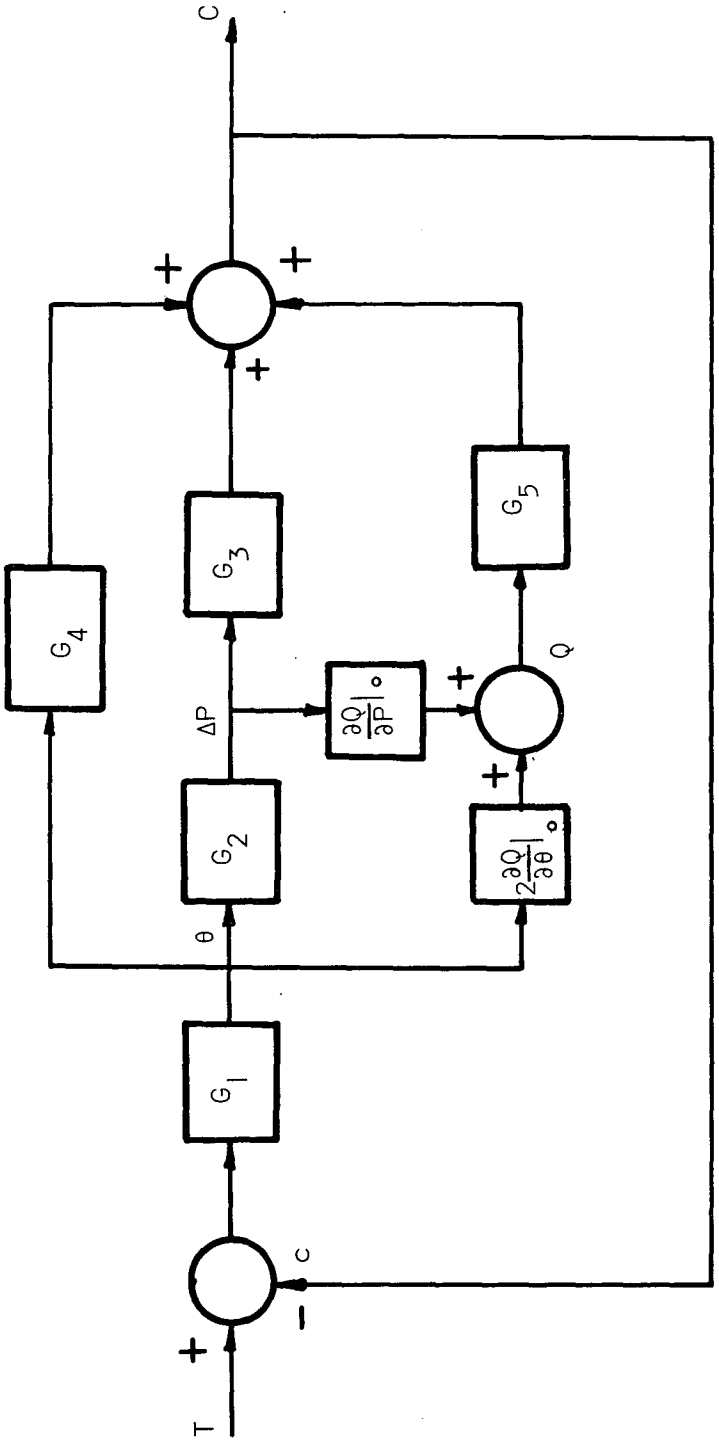

Figure 10 Block Diagram of the High Temperature Breadboard Model

line effects of a length of tubing could be used as a damper on the flapper. The other departure was made when it was found that the loop gain was sufficiently high, without additional amplification, for the beam deflection amplifiers to be eliminated. However, before these two discoveries, an amplifier had been designed and tested [9]. The results are of sufficient interest to warrant a brief description of the results.

The amplifier was machined from a block of RA 330 stainless steel with a top plate being attached by oven brazing. The important dimensions are shown in Fig. 11. The system was tested for static performance in a temperature controlled oven. Results were plotted in the form of input and output flow curves. From these, lumped parameters were obtained. The parameters are shown in Table II for various temperatures to 2000°F. These parameters were then used in an analog linear model to calculate the frequency response. The actual frequency response was then determined experimentally, using a wobble plate signal generator for low frequencies and a notched plate generator for high frequencies. The results for room temperature and for 2000°F are shown in Fig. 12. The lines represent the linear model and the experimental data are shown as points. The linear model tended to represent the magnitude ratio best at low temperatures and the phase angle best at high temperatures. The static curves were also used to derive transfer curves. These are shown in Fig. 13.

The second departure from the original system plan involved the use of the transmission line damper for compensation. A schematic of this system is shown in Fig. 14. Effectively, motion of the flapper causes a change in the flow and pressure at the nozzles. There is a lag in the transmission of the pressure wave around the loop. The result is that the pressures on either side of the flapper are out of phase with the flapper motion and thus give a damping effect.

Equations for the damper were written using transmission line theory. With the assignment of boundary values the equations can be written in the form of a Laplace transform for displacement of the flapper as:

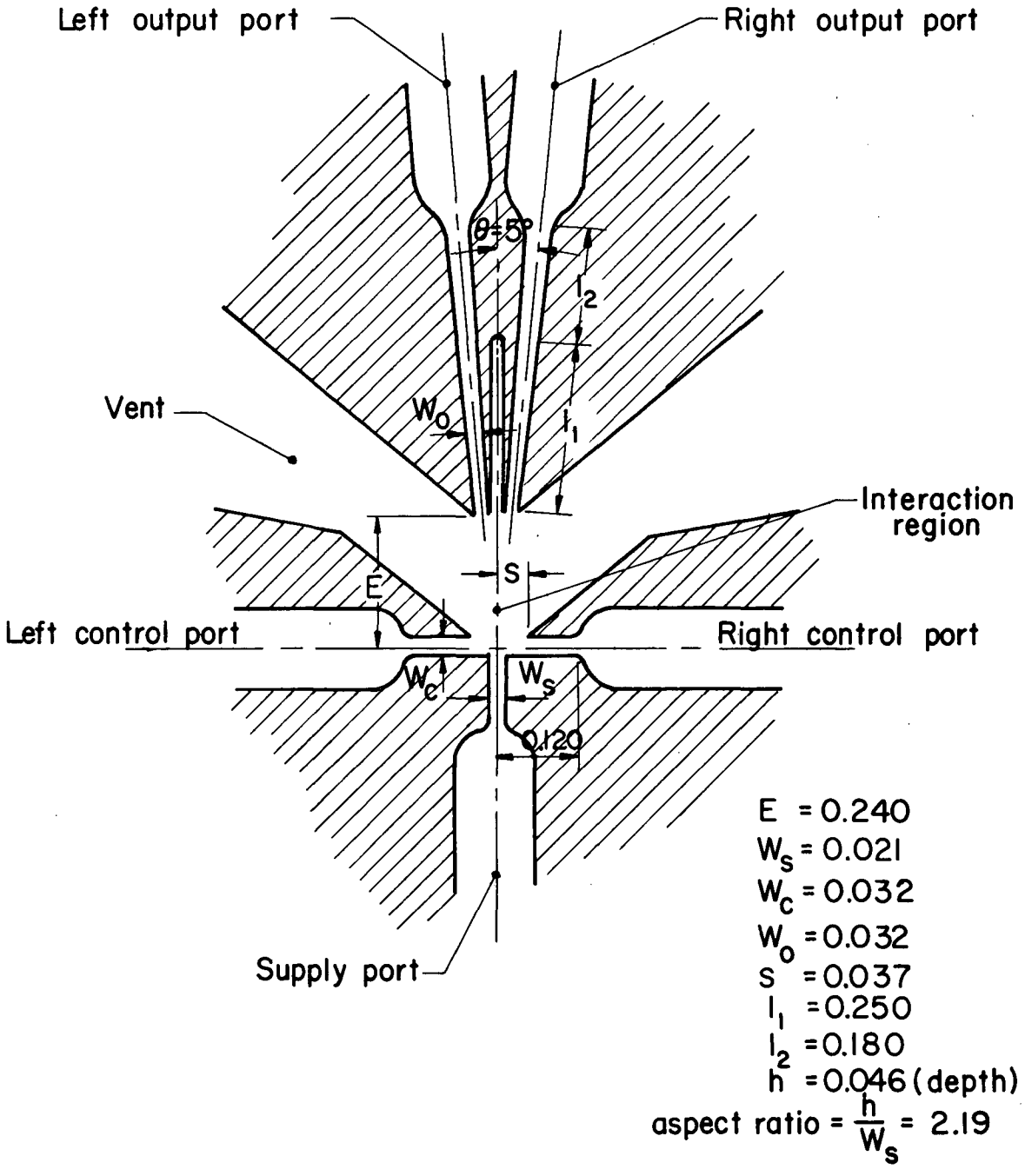

Figure 11 Amplifier Main Dimensions

TABLE 2

AMPLIFIER PARAMETER VALUES

Parameter	Temperature °F					
	70	500	1000	1500	1800	2000
Input resist.						
$R_C \left[\frac{lb\ sec}{in^5}\right]$	0.33	0.26	0.22	0.18	0.18	0.19
Output resist.						
$R_o \left[\frac{lb\ sec}{in^5}\right]$	0.25	0.20	0.16	0.11	0.11	0.075
Input capac.						
$C_C \left[\frac{in}{lb}\right] \times 10^5$	0.80	0.80	0.80	0.80	0.80	0.80
Output capac.						
$C_O \left[\frac{in^5}{lb}\right] \times 10^5$	4.68	4.75	4.79	4.86	4.89	4.89
Presure gain						
G	5.18	4.98	4.20	3.90	3.20	2.90
Pressure amplification factor						
K_p	3.70	4.21	4.30	4.60	4.62	4.70
Total time delay						
t_d [sec] $\times 10^3$	0.17	0.14	0.14	0.065	0.066	0.066

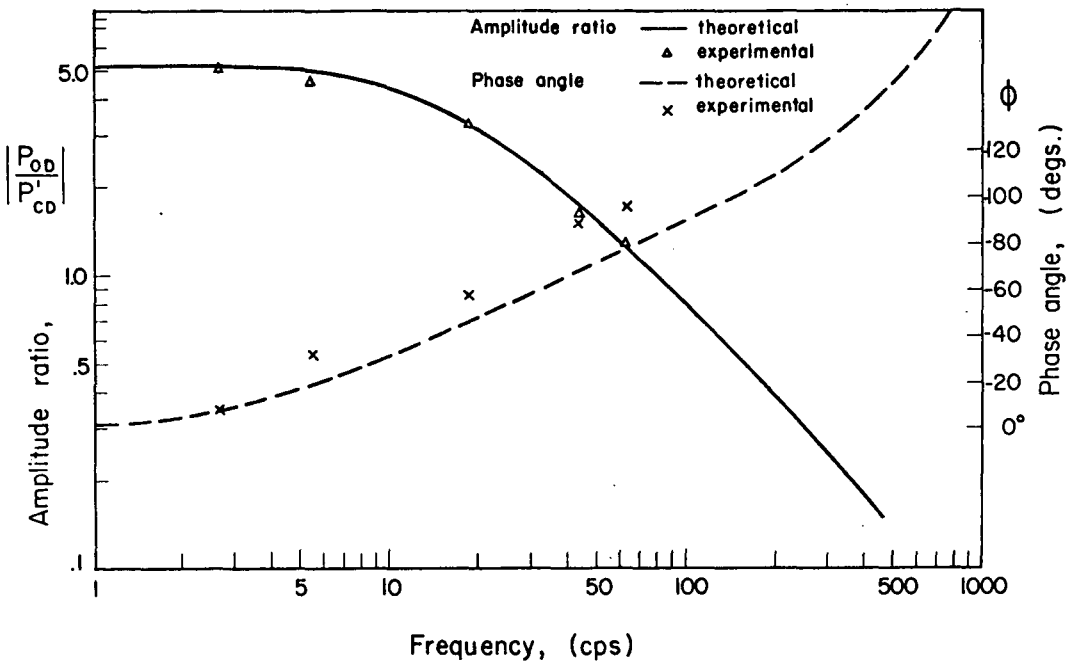

Figure 12A Frequency Response (70°F)

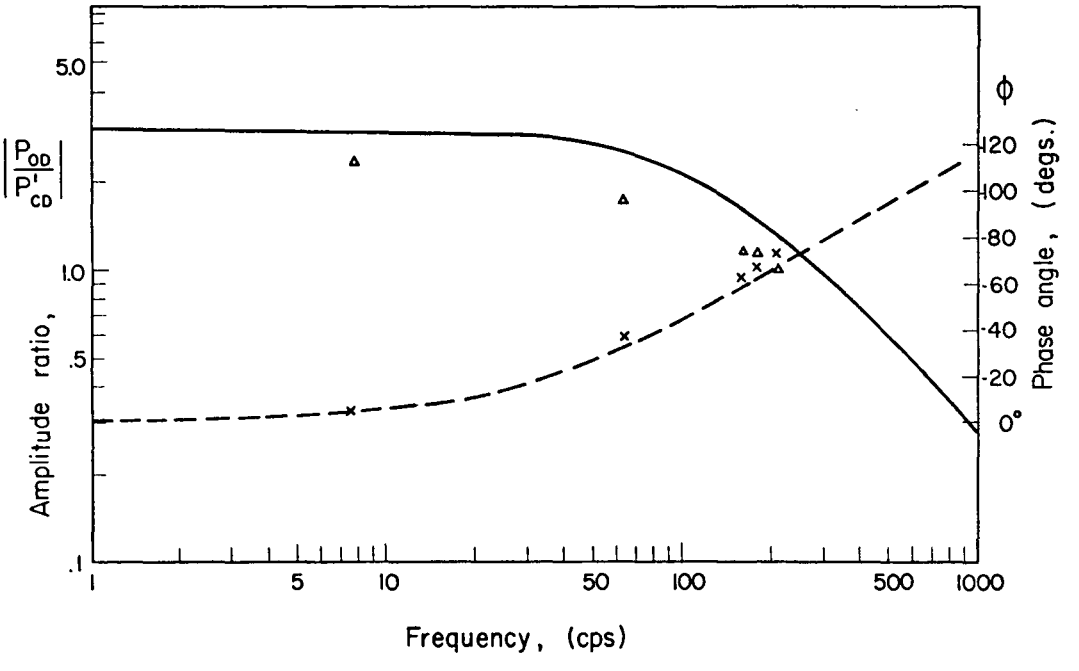

Figure 12B Frequency Response (2000°F)

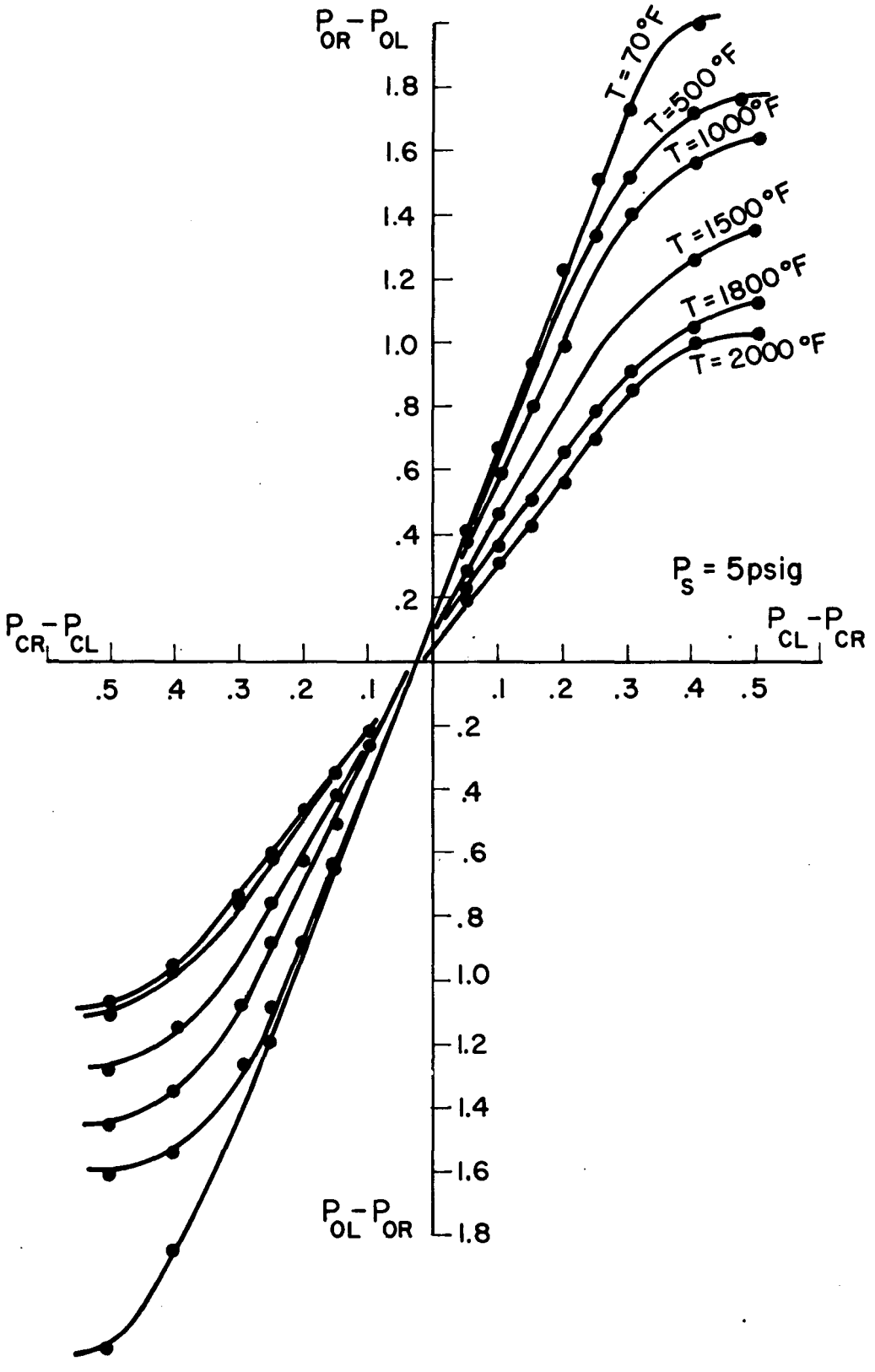

Figure 13 Transfer Characteristics - Variable Temperature (P_S = 5 psig)

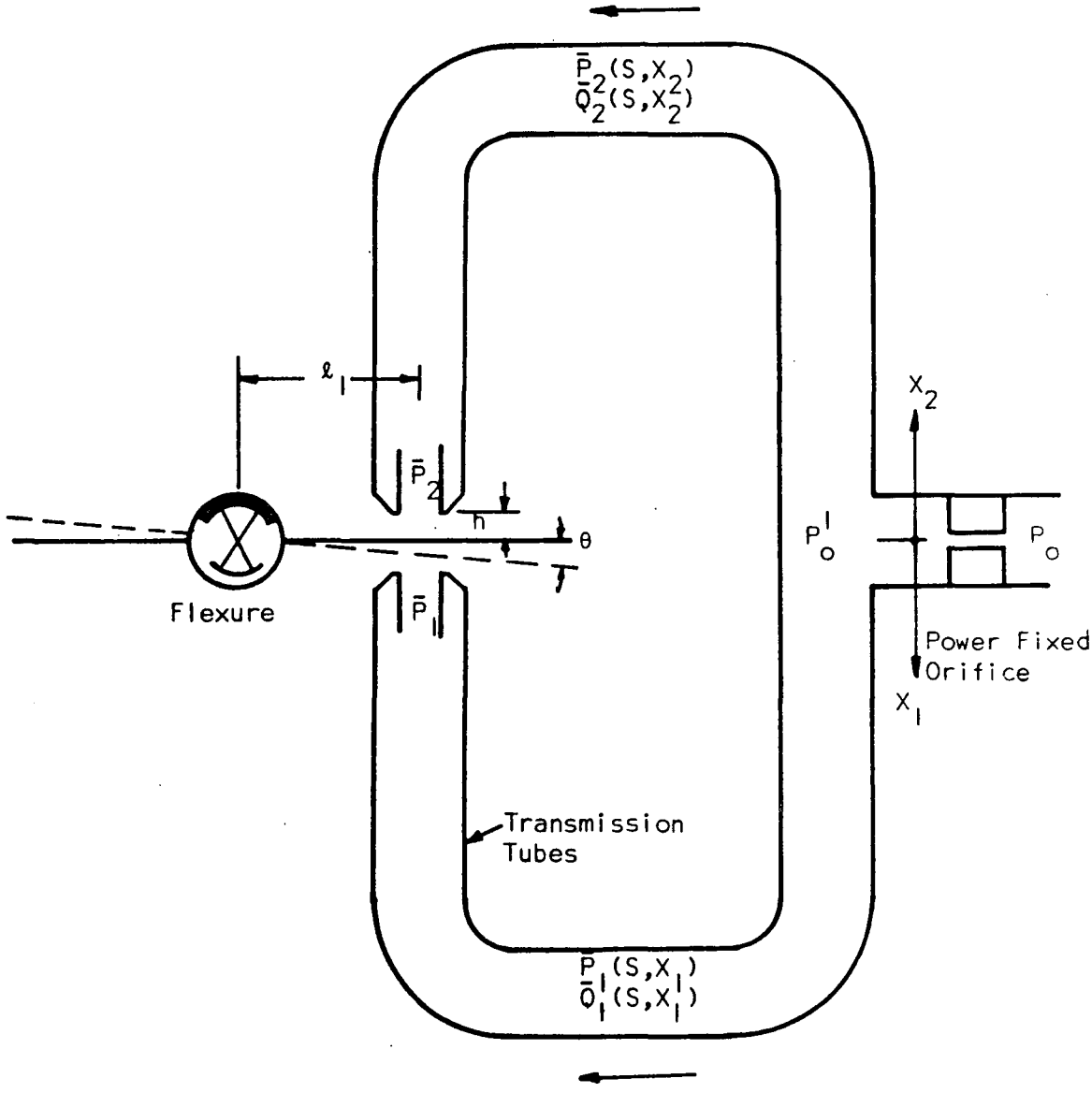

Figure 14 Sketch of the Pneumatic Damper

$$\theta(s) = \frac{Is\theta(o) + I\theta'(o) + T_o(s)}{Is^2 + K + K_1 + \dfrac{K_2 \dfrac{\partial Q}{\partial \theta} Z_o(s)\sinh \lambda \ell - K_3 \dfrac{\partial Q}{\partial \theta} \dfrac{\cosh \lambda \ell}{Z_c(s)}}{\cosh \lambda \ell + Z_c(s) \dfrac{\partial Q}{\partial P} \sin \lambda \ell}} \qquad (7)$$

Equation 7 was solved using a digital computer. Comparison was made with test results for a number of different supply pressures, nozzle gaps, and transmission line lengths. Figure 15 shows a typical response for a step input in torque to the flapper. Approximation of the hyperbolic functions by infinite products and retention of only the most significant terms yields:

$$\theta(s) = \frac{[Is\theta(o) + I\theta'(o) + T_o(s)][a_4 s^4 + a_3 s^3 + a_2 s^2 + a_1 s + a_0]}{[b_6 s^6 + b_5 s^5 + b_4 s^4 + b_3 s^3 + b_2 s^2 + b_1 s + b_0]} \qquad (8)$$

Solution of this equation for the roots and the results of the experimentation shows that an adequate model could be obtained using a second order equation. For example, an adequate representation is

$$\frac{\theta}{T}(s) = \frac{0.28s + 1500}{(s + 30 \pm 85j)} \qquad (9)$$

for a supply pressure of 5 psi and a nozzle gap of 1.5 mils.

The damper, flapper valve, and motor combined give the transfer function of Eq. 6. A breadboard model of this system was built and tested to 2000°F. It is shown after testing in the photo of Fig. 16. The central portion of the device contains the flexure-mounted flapper and nozzles. The other rectangular elements are capacitance tanks. Pressure and flow were measured outside the test oven. Temperature was measured with thermocouples mounted within the capacitance tanks.

Extensive data was obtained for many different values of the various system variables. A few examples are shown here. Figure 17 is typical of curves obtained for nozzle chamber pressure vs. deflection with temperature as the variable. Combination of this characteristic with that of

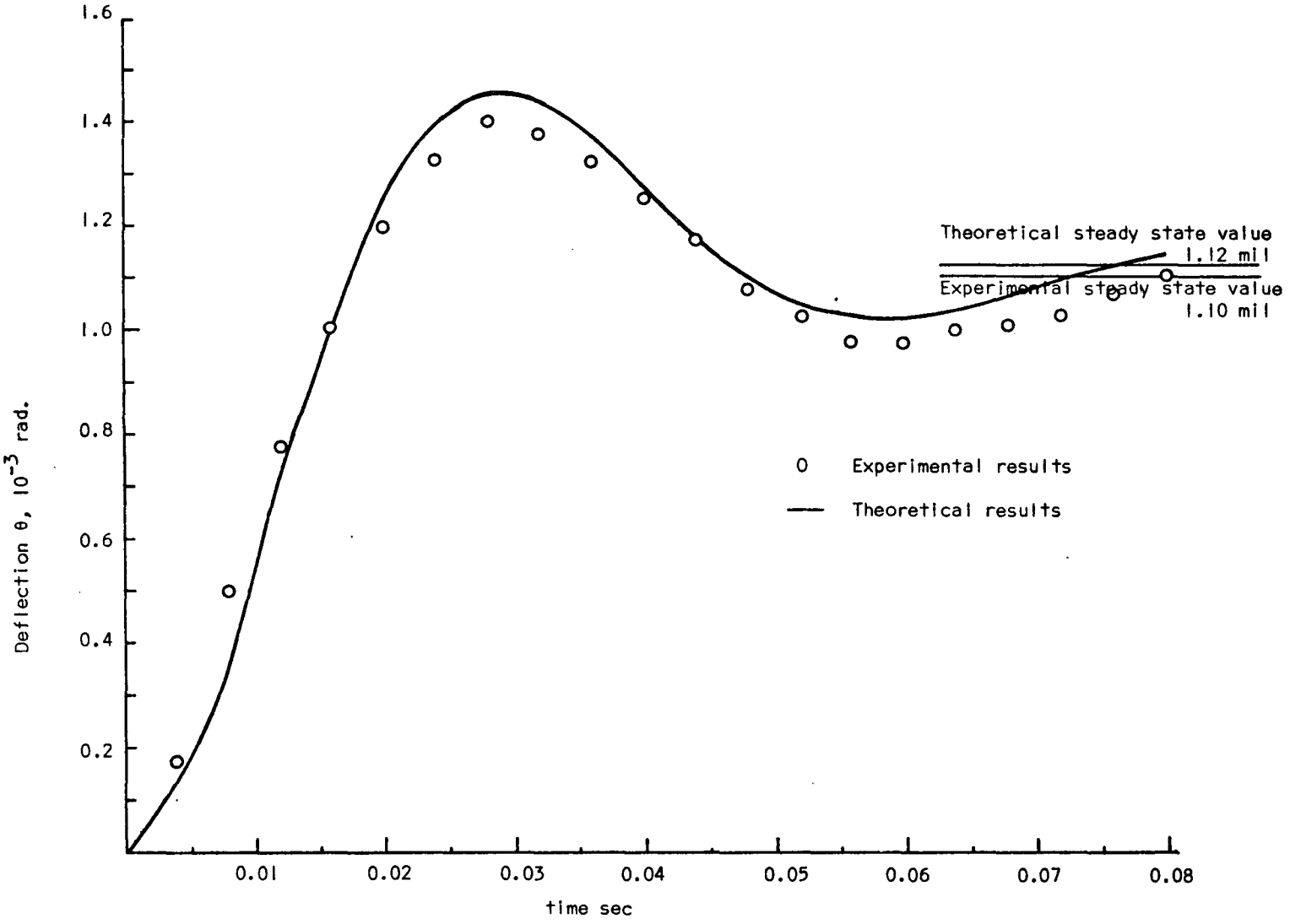

Figure 15 The Theoretical and Experimental Results of the Response on a Pneumatic Damper to a Step Input, P_o = 8 psig, h_o = 1.5 x 10^{-3} inch

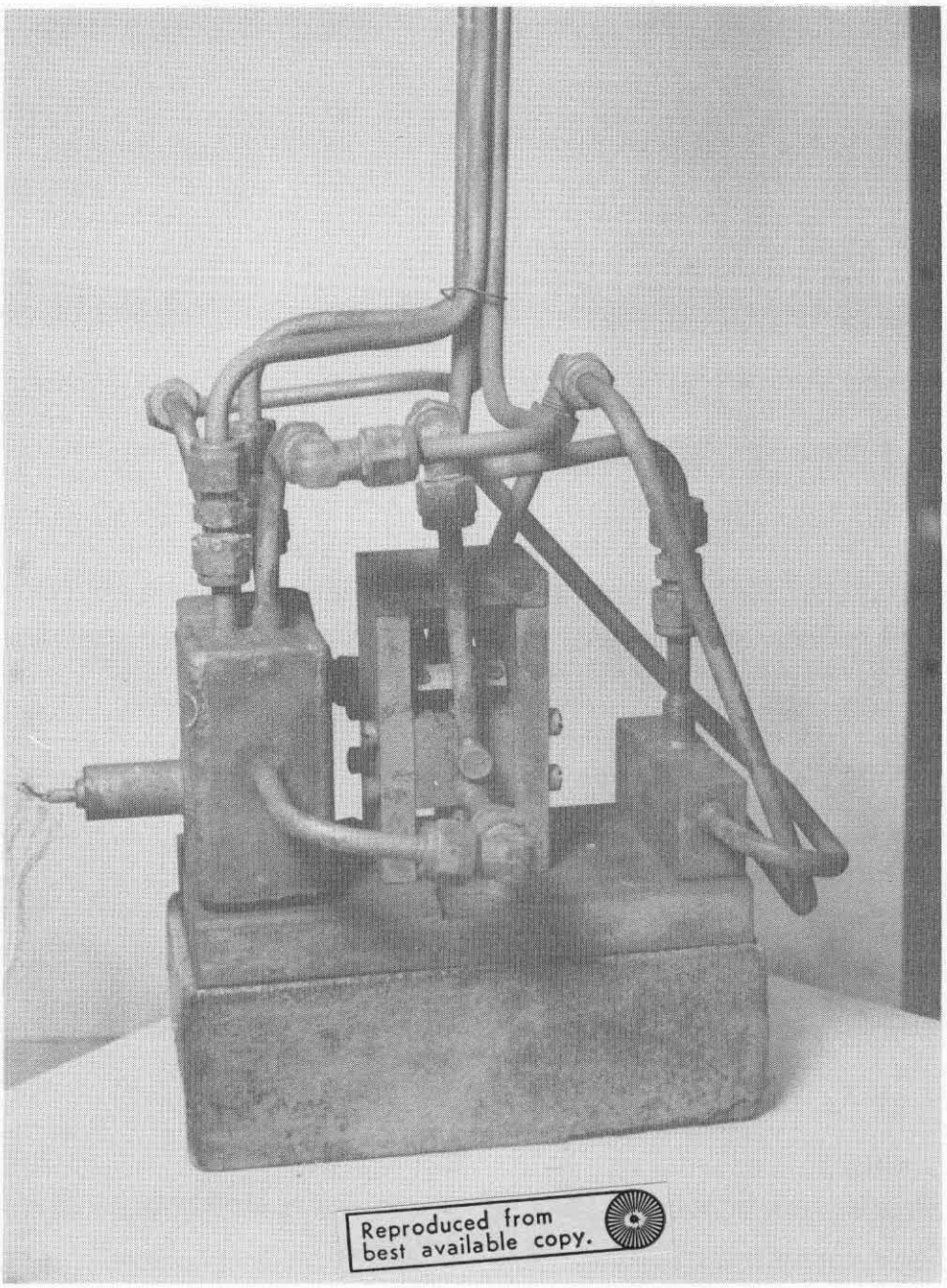

Figure 16 High Temperature Breadboard Model

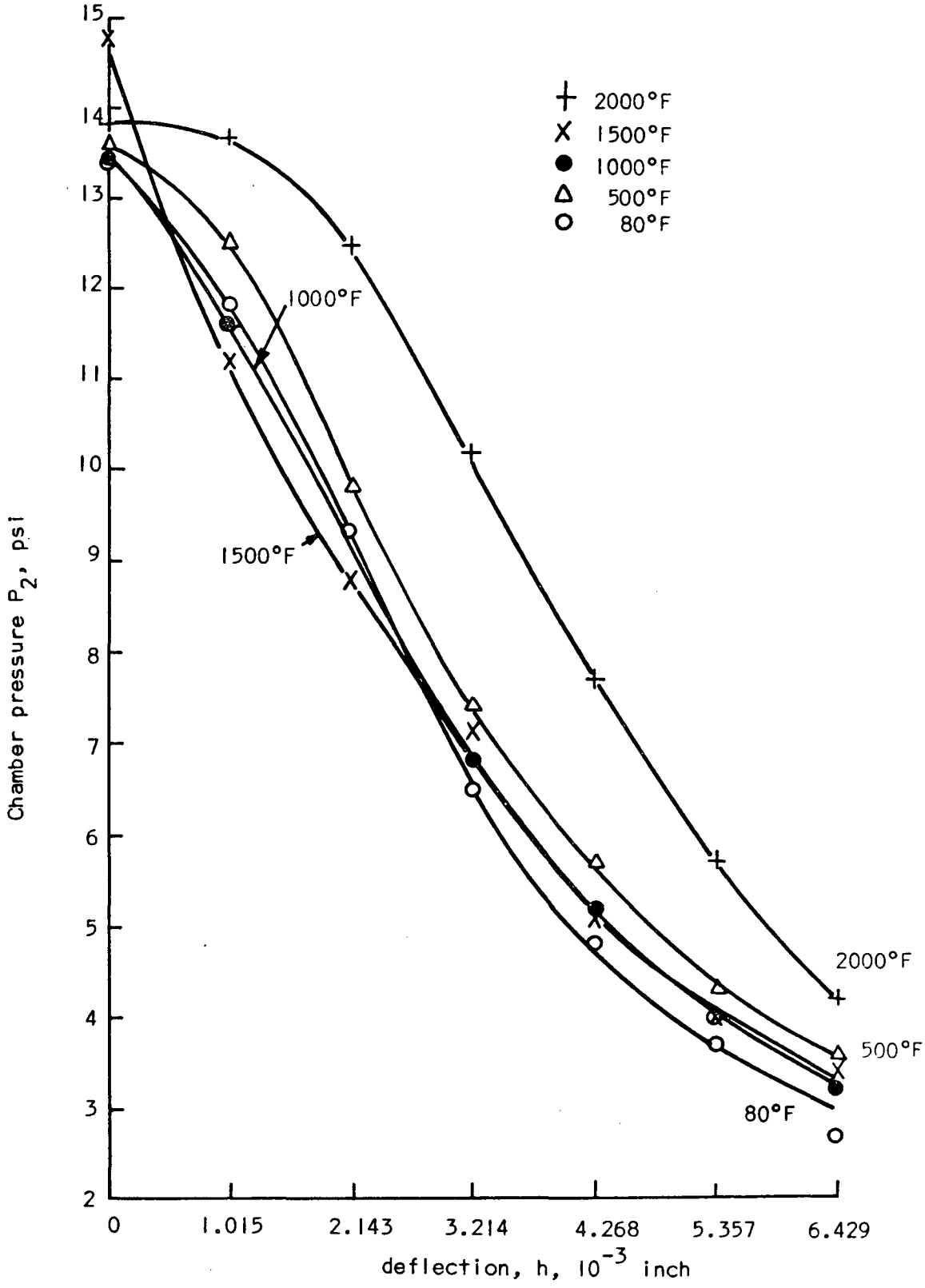

Figure 17 Chamber Pressure, P_2, as a Function of Displacement for P_1 15 psig

an opposing nozzle gives good linearity over a range of about 2 mils, which is far more than adequate for application in the drag sensor.

Figure 18 shows the response of the sensor to step changes in torque (drag force on the target). These curves were traced from oscilloscope pictures.

The ultimate goal of the sensor is the detection of skin friction drag force in terms of ΔP. Typical results for these terms are shown in Fig. 19. It is seen that excellent linearity is obtained at fixed temperatures over a range of almost three times the range required in the design specifications. Use of the sensor for accurate measurement would require temperature sensing unless some temperature compensation were included in the control system. One possible approach to this lies in making the supply pressure vary in proportion to temperature. In Fig. 19 the slopes of the curves decrease with increasing temperature. When the supply pressure is increased the slopes increase and linearity is maintained so the effects may possibly be used to cancel each other. This possibility has not yet been explored.

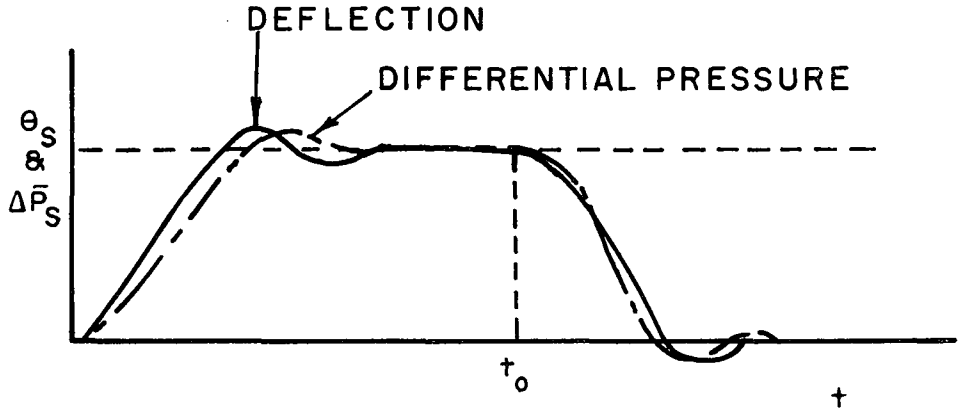

Figure 18 A Long Square Wave Serves as the Initial Condition

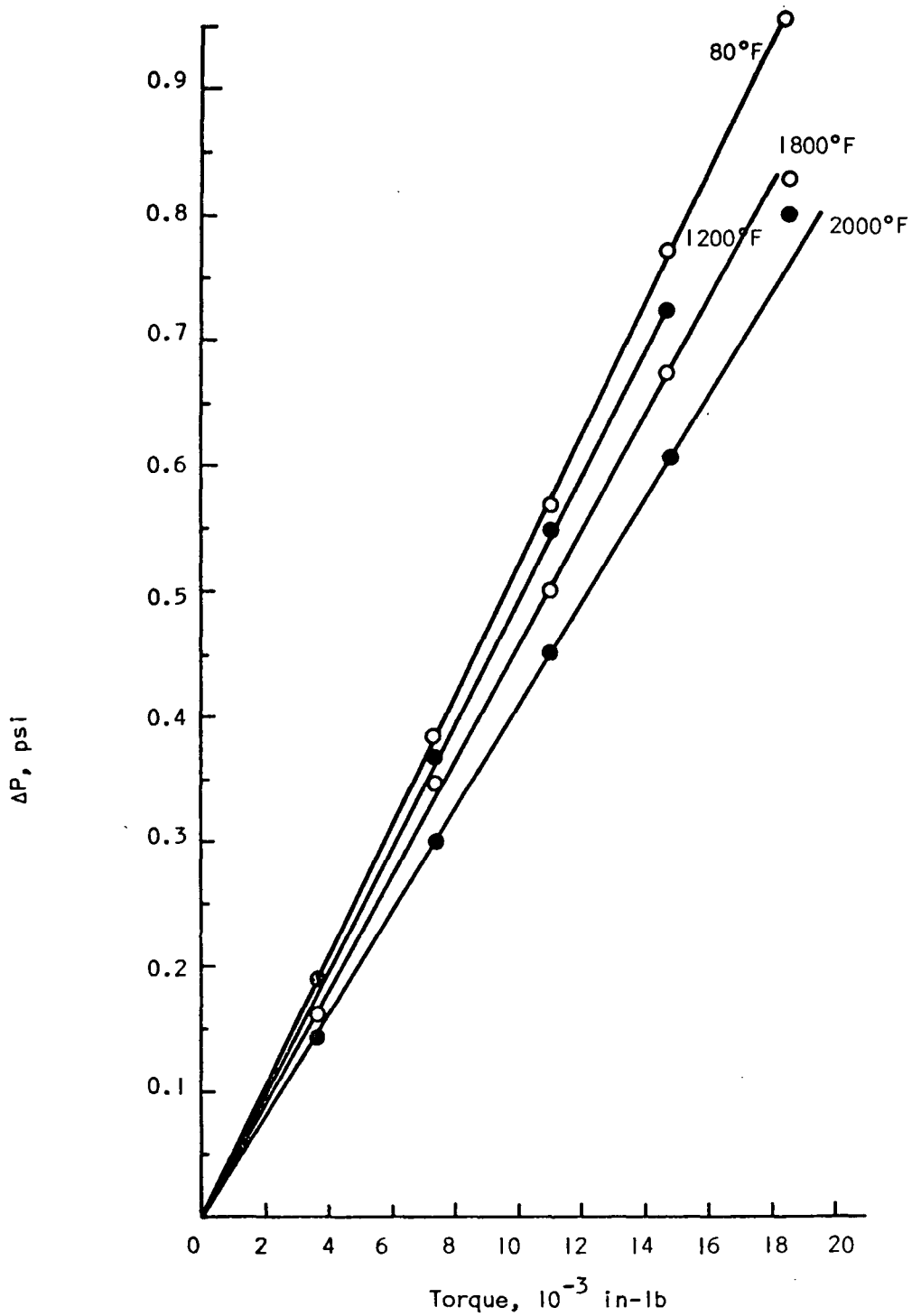

Figure 19 Modified Differential Pressure Versus Torque Relations for the Closed Loop System, P_1 = 10 psig

SECTION IV

SUPPORT SYSTEM

The environmental specifications are the same for the support system as for the control system. The requirements are that the sensor be insensitive to temperature and to translational and rotational accelerations. Experiments have been performed using two basic approaches. One approach uses spherical gas bearings [10] and the other uses flexure pivots [11].

To make the system insensitive to acceleration it must be counterbalanced in rotation and translation. This is done by using balanced contra-rotating cylinders as shown schematically in Fig. 20. Contra-rotation is obtained by using tension bands between the two cylinders. As shown here the support of each cylinder is the equivalent of a three element flexure pivot with the third element replaced by the interconnecting bands. The same arrangement is used to make the gas bearing support insensitive to acceleration, the gas bearing merely replacing the flexures in support of the two cylinders.

Flexure pivots have a rotational spring constant. Three-flexure pivots have the advantage that the rotational constant can be adjusted by adjusting the tension in the flexures. Another advantage is that the rotational spring constant is not affected by translational accelerations.

Results of room temperature testing using various flexure tensions are shown in Fig. 21. The curves show that for higher values of tension the rotational constant becomes negative. The early curves, through No. 5, were not adjusted for null shift under the increasing tension.

An extensive computer program has been developed for dynamic studies treating the system of Fig. 20 as a six degree of freedom system. Results have been used to select the flexure dimensions and to optimize the initial tension to give satisfactory performance over the required temperature and acceleration range.

The gas bearing support has been tested in an oven to 2000°F using a single cylinder and two hemi-spherical bearings. The bearings were

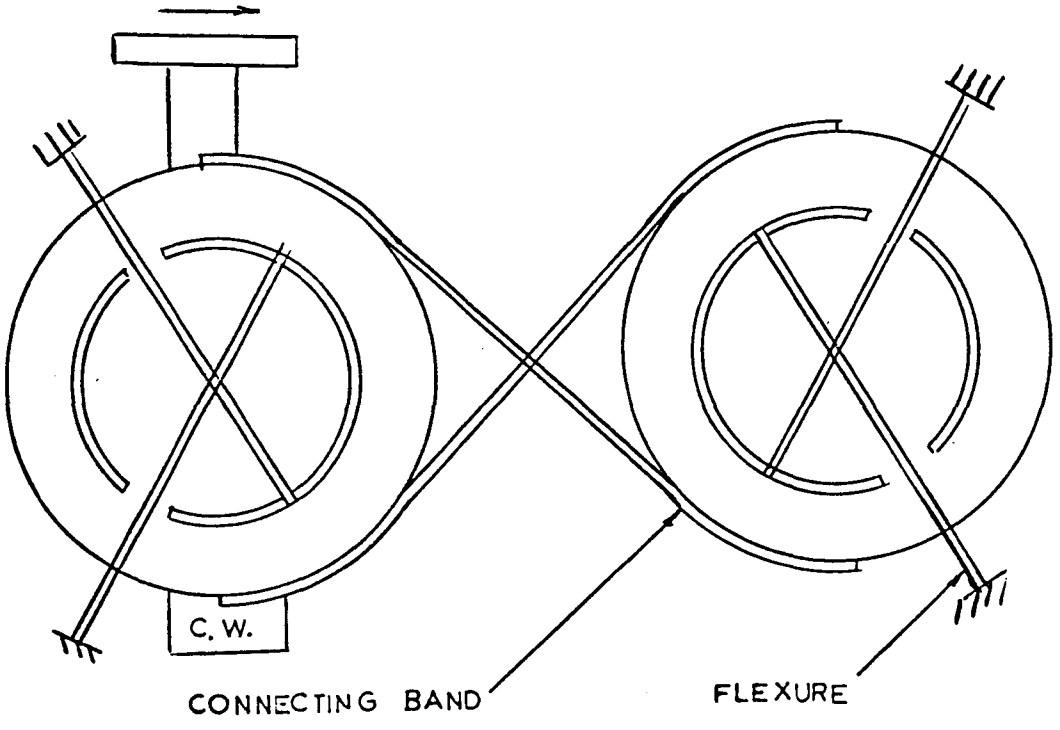

Figure 20 Counterbalancing System Using Flexure Construction

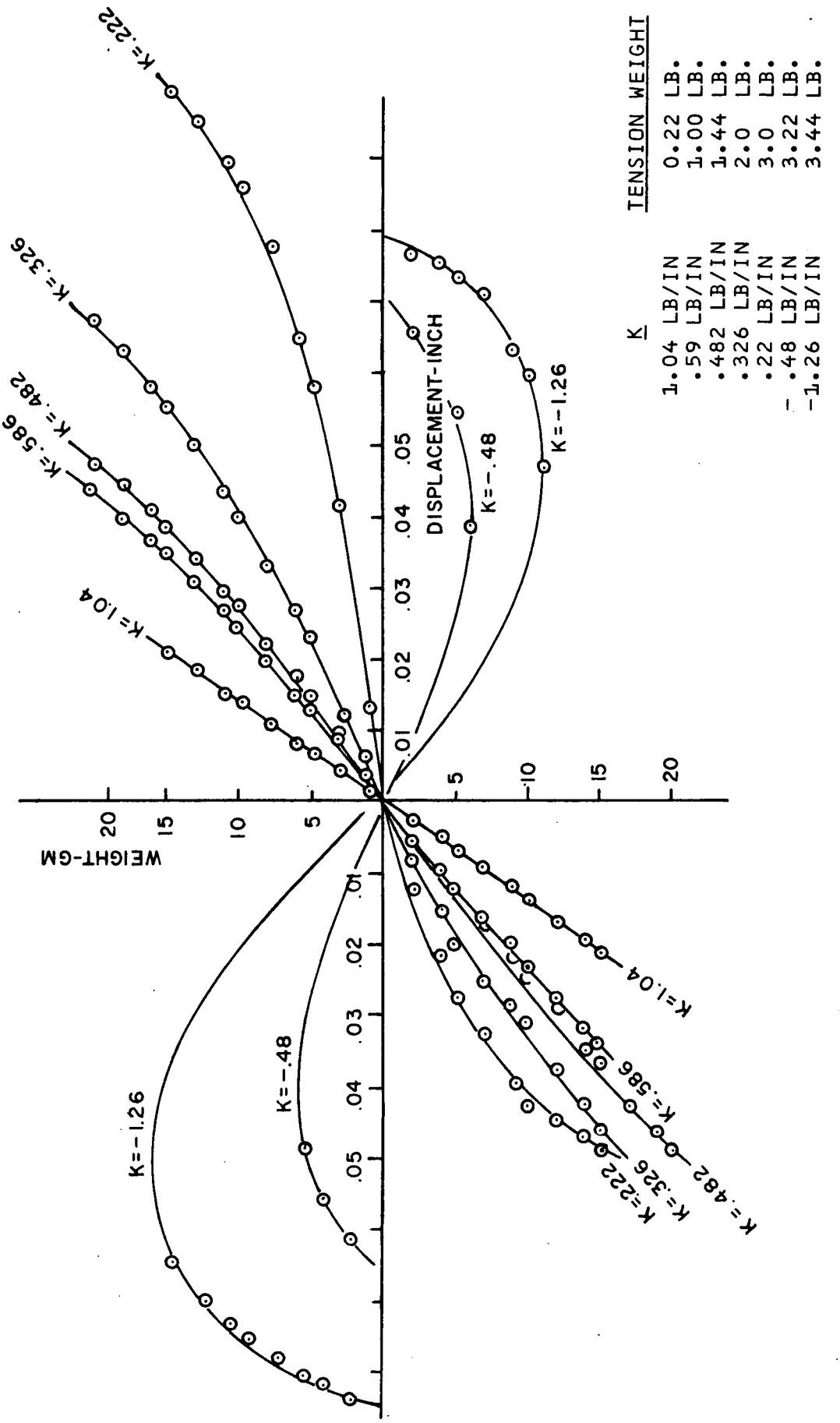

Figure 21 Force Vs. Displacement for Various Tensions

made from ordinary steel bearing balls by electrostatic discharge machining of three pressure pads on the support side. The rotating element sockets were made by grinding another bearing ball as a cutting tool and then lapping to final dimensions. Nitrogen was used as the working fluid. Over the temperature range the bearing maximum load capacity decreased from 2.5 lbs at room temperature to 1.8 lbs at 2000°F, using 100 psi supply pressure. Over the same range the stiffness decreased from 1520 lb/in to 850 lb/in.

All test results to date have been satisfactory although a complete counterbalanced support system has yet to be tested. Both the electrical and pneumatic systems have used two-flexure supports, non-counterbalanced, for the breadboard testing. These have been constructed of natural ceramic material, using RA 330 stainless steel or Haynes Alloy No. 25 as the flexure materials. These have withstood many hours of high temperature testing.

The system delivered to NASA is not capable of being operated in a severe vibrational environment. This area needs the remaining available effort. Thus the remaining time will be spent on analysis and design of the counterbalanced support system. Available resources will not permit implementation of the design, so emphasis will be placed on presenting the information in a manner to allow the sponsor to complete the project with a minimum of effort.

Several other aspects which were studied during this research work, but which were not carried to completion due to lack of resources, are deserving of further research. These are:

1. Air bearing support system.
2. Cobalt motor.
3. Pneumatic system.

Operating instructions for the completed system are in Appendix A, and final data are in Appendix B.

SECTION V

CONCLUSIONS AND FUTURE WORK

Feasible solutions to the problem of making inflight measurements of skin friction have been presented. One of the three feasible approaches has been developed to the prototype stage for wind tunnel testing and is presently being placed in service by the sponsor. Successful operation of both pneumatic and electrical systems has extended the motor-sensor technology for ultrahigh temperature operation.

LIST OF REFERENCES

1. Weiler, John Eugene, Sr., "Design of an Acceleration Insensitive Skin Friction Balance for Flight Testing," Master Thesis, The University of Texas, Austin, June 1954.
2. "Conceptual and Preliminary Design of the Hypersonic Ramjet," Statement of Work, Exhibit AL-4947, April 15, 1965, Langley Research Center, Langley Station, Hampton, Virginia.
3. Ashby, Richard G., "The Counterbalancing of Accelerations in a Skin Friction Meter," Master's Thesis, The University of Virginia, Charlottesville, Virginia, August 1968.
4. Fenter, Felix W., and Lyons, W. C., Jr., "The Direct Measurement of Local Skin Friction on Aerobee-Hi Rockets in Free Flight," The University of Texas, Austin, Texas, DRL-391, CM-877, 16 May 1957.
5. "Kistler Skin Friction Drag Sensor," Files of Force Measurements Group, Instrumentation Research Division, NASA, Langley Field, Virginia.
6. McVey, E. S., Moore, J. W., "A Force Balance System for the Measurement of Skin Friction Drag Force in the Presence of Large Vibrations and Temperatures," Report No. EME-4029-109-69U, September 1969, Research Laboratories for the Engineering Sciences, University of Virginia, Charlottesville, Virginia.
7. Kettler, D. A., "The Design of a High Temperature Skin Friction Meter System," Master of Science Thesis, University of Virginia, Charlottesville, Virginia, December 1969.
8. McVey, E. S., Moore, J. W., and Lu, C. S., "A Force Balance System for the Measurement of Skin Friction Drag Force," Report EME-4029-111-70U, Research Laboratories for the Engineering Sciences, University of Virginia, Charlottesville, Virginia, April 1970.
9. Sabella, Hector M., "Elevated Temperature Effects on a Proportional Fluidic Amplifier," Master's Thesis, The University of Virginia, 1970.
10. Schilbe, A. L., Jr., "Design and Evaluation of a Gas Bearing Support for a Skin Friction Meter," Master's Thesis, University of Virginia, 1969.
11. Ho, Domingo Tan, "Design of a Flexure Pivot System with Low Sensitivity to Accelerations," Master's Thesis, University of Virginia, 1970.

APPENDIX A

1.0 INTRODUCTION

1.1 General

The skin-friction meter described in this manual was delivered to the Instrument Research Division, NASA Langley Research Center and developed under NASA Grant NGR 47-005-026. This meter is a complete measurement system designed to measure forces in the range of 0.7 to 7 millipounds (0.157×10^{-3} to 1.57×10^{-3} newtons) in sustained ambient temperatures up to 2000°F (1093°C) with a maximum steady-state target deflection of 0.5×10^{-3} inch (12.7×10^{-3} millimeter).

The meter is a force-balance system consisting of two separate units--a motor-sensor with attached target and an electronics package. The motor-sensor unit is mounted on the surface to be tested with the target becoming a part (with a small air gap) of the wall along which the gas flows. The electronics package is mounted away from the high temperature environment and connected to the motor-sensor by six leads.

1.2 Documentation

This manual is intended to be a guide to the installation, use, and repair of the skin-friction meter. A detailed discussion of the theory and operation is contained in Report No. EME-4029-110-70U of the Research Laboratories for the Engineering Sciences, University of Virginia, Charlottesville, Virginia. This is a quarterly progress report of NASA Grant No. NGL 47-005-026.

1.3 Principles of Operation

The skin-friction meter is shown schematically in Fig. A-1. The target and motor armature (which also serves as the sensor rotor) are supported by the flexure and are free to rotate about the flexure restrained only by the motor and spring constant of the flexure. Gas flow along the wall of the test section causes a force on the target resulting in a displacement. This displacement is detected by the displacement transducer which produces a voltage proportional to the displacement. This error

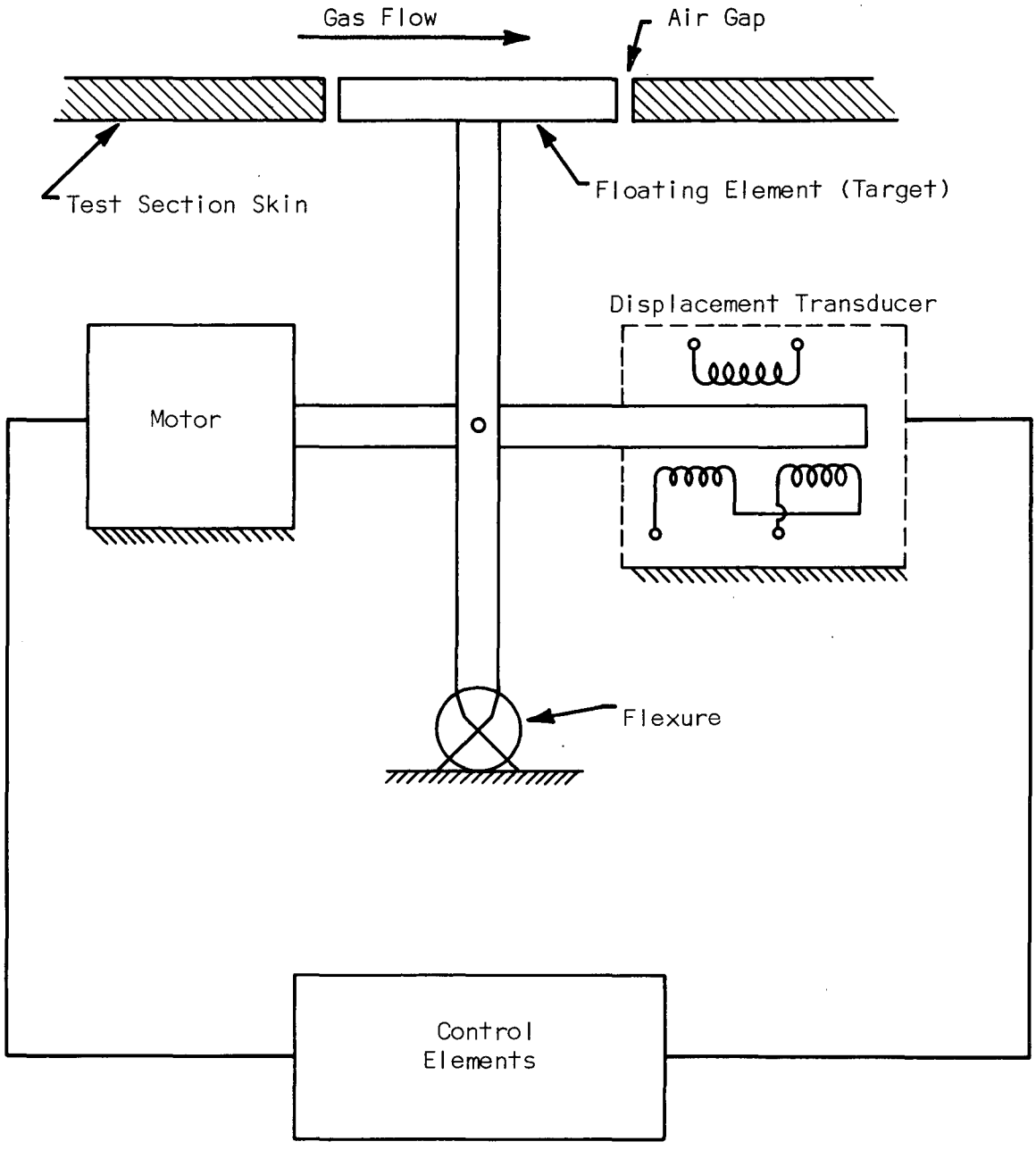

Figure A-1 Schematic Diagram of Closed Loop System for Measuring Skin Friction

voltage is then amplified by a power amplifier and applied to the motor armature causing a restoring torque. The force measurement is obtained by reading the armature current because the motor torque is proportional to the armature current for this type of motor.

The motor for the skin-friction meter consists of an armature coil positioned inside and between two separate field coils as shown schematically in Fig. A-2. The field coils are driven by two separate constant current sources, and these currents set up a magnetic field parallel to the armature coil plane. When current is passed through the armature coil, the motor produces a torque proportional to the armature current and whose direction depends upon the field coil and armature coil current directions.

The displacement transducer was shown separated from the motor in Fig. A-1 for clarity of illustration, but actually it uses the same components as the motor. The armature coil is driven by a 5 KHz carrier signal provided by a constant-amplitude constant-frequency signal generator and power amplifier. This carrier signal is inductively coupled to the separate field coils and induces a 5 KHz signal on the field coils. The signals from the two field coils are added and demodulated, and the amplitude of the resulting signal indicates the magnitude of the deflection. This signal is the error signal and is used to control the armature current.

2.0 ELECTRONIC CONTROL CIRCUITS

2.1 Description of Closed-Loop Operation

A block diagram of the skin-friction meter is shown in Fig. A-3. The 5 KHz carrier signal generator is amplified by the power amplifier and applied to the armature coil through the flexure. This carrier is then inductively coupled to the two field coils. If the skin-friction meter has no force on it, the axes of the armature and field coils are perpendicular to each other, and no voltage is induced across the field coils. However, if a force is exerted on the test section causing a rotation of the armature coil, then the axes of the coils are not perpendicular and a voltage is induced across the field coils.

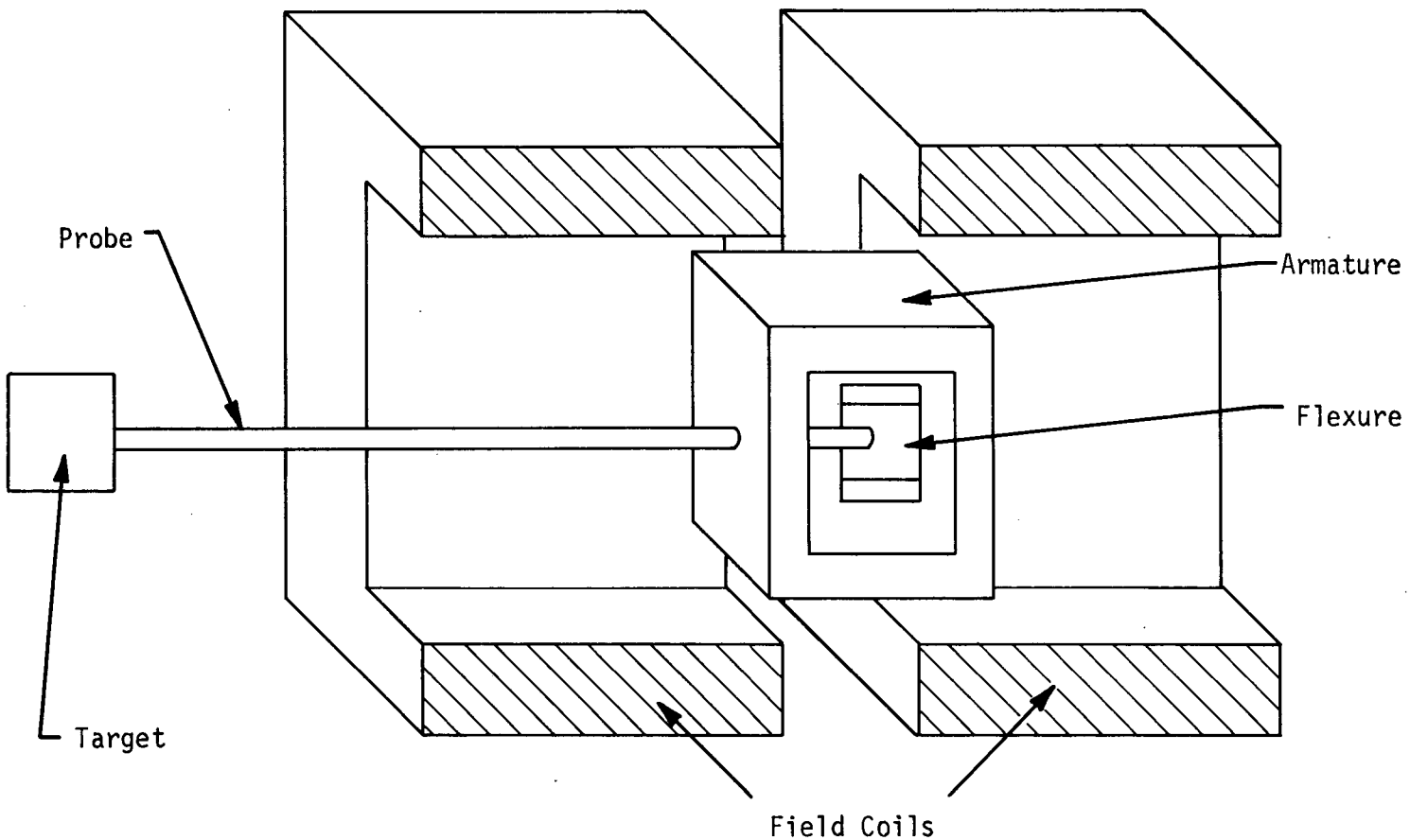

Figure A-2 Sketch of Motor-Sensor

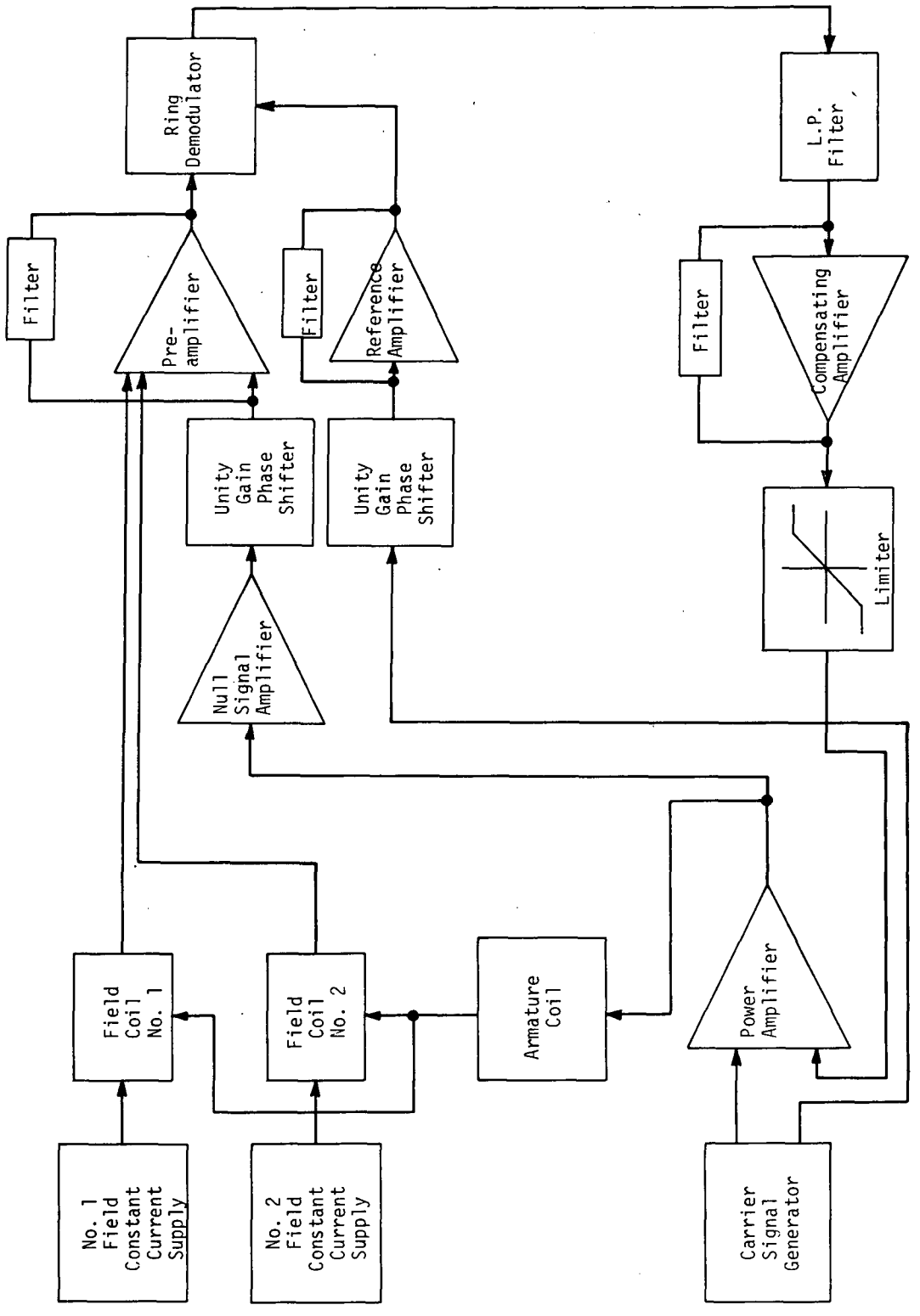

Figure A-3 Block Diagram of the Closed Loop System

The outputs of the field coils are a-c coupled, summed, filtered, and amplified by the preamplifier. A null signal is also inserted at this point to correct small physical misalignments.

The output of the preamplifier is then fed into one of the inputs of a ring demodulator. The other input to the demodulator is a reference signal derived from the carrier generator through an amplifier and adjustable phase shifter. The output of the demodulator is a d-c voltage (with a very small 5 KHz ripple) whose magnitude is proportional to the deflection of the target.

The demodulator output goes into the compensating amplifier where it is amplified, and closed-loop frequency compensation is applied. This is then fed into a limiter which prevents turn-on transients from saturating the power amplifier. The output of the limiter is then fed back into the power amplifier, where it is combined with the 5 KHz carrier signal, to produce the current in the armature to null the applied force.

The remaining components of the system are the two field coil constant-current sources. These maintain a constant current through the field coils despite temperature changes (and resultant resistance changes) in the field coils.

2.2 Component Descriptions and Specifications

This section contains a more detailed description of the individual components of the skin-friction meter. The complete electrical schematic is shown in Fig. A-4 where the individual components are enclosed in dashed lines and labelled.

2.2.1 Carrier Signal Generator

The carrier signal generator is a commercial sine wave oscillator, and is not furnished with the skin-friction meter. Any high quality signal generator that will provide a relatively constant-frequency constant-amplitude 5 KHz sine wave of amplitude greater than 200 millivolts should be satisfactory. A Hewlett-Packard Test Oscillator 651A was used for all testing.

All resistors 1/2 watt unless otherwise indicated
All resistances in ohms
All capacitances in microfarads unless otherwise indicated
±15-volt supplies are type Hewlett-Packard Model 721A
±30-volt supplies are type Harrison Lab Model 6433B
Signal generator is Hewlett-Packard Test Oscillator 651A

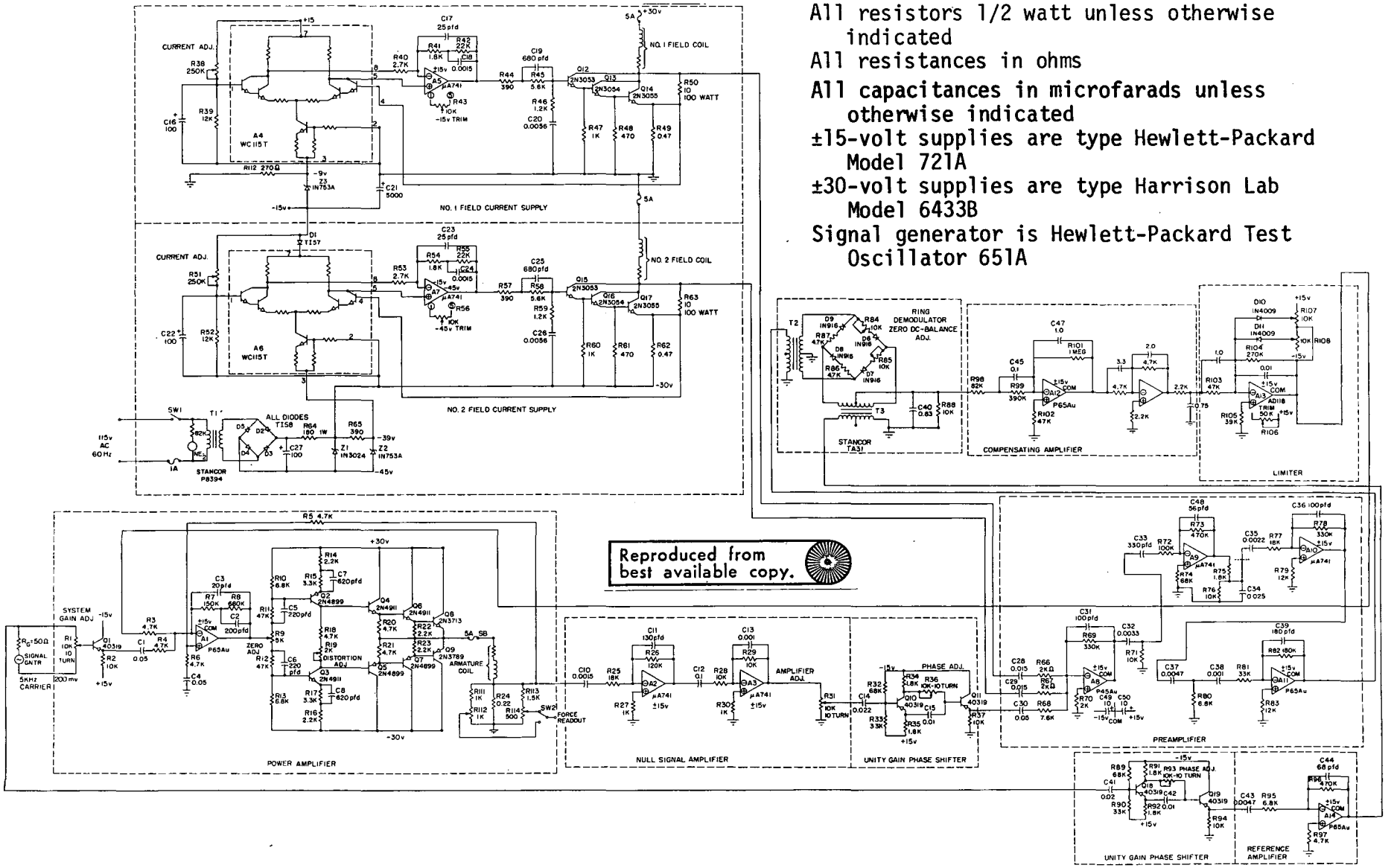

Figure A-4 Electrical Schematic of Skin-Friction Meter

2.2.2 Power Amplifier

The first section of the power amplifier consists of a system gain adjust potentiometer, R1, and an emitter follower buffer. The next section of the power amplifier is an operational amplifier and associated components that sums the carrier and error signals and subtracts the amplifier feedback signal. The feedback is derived from the voltage across R24 which is in series with the armature coil. R24 is also used to provide the force read-out with suitable range trimming potentiometers R114 and R112 for the high and low ranges respectively. The high range provides 0 to 100 millivolts for 0 to 7 millipounds force, and the low range provides 0 to 100 millivolts for 0 to 0.7 millipounds. The remainder of the power amplifier is a standard complementary-symmetry direct-coupled power amplifier using split power supplies.

The power amplifier can be characterized as a component with a summing input, a voltage to current transconductance of 4.54 amps per volt input for the error and carrier signals with a double pole at 20 KHz. Adjustments are also provided to zero the output and minimize the crossover distortion.

The power supply requirements for the power amplifier are ± 30 volts at 5 amps and ± 15 volts at 20 milliamps. There is a 5 amp slow blow fuse in the output to protect the amplifier if the output is inadvertantly shorted.

2.2.3 Preamplifier

The preamplifier for the nulled 5 KHz carrier signal is a four stage amplifier consisting of amplifiers A8, A9, A10, A11, and their associated circuitry. The preamplifier provides an overall gain of 7000 and has a limited passband characteristic centered at the carrier frequency of 5 KHz. The filtering was necessitated by serious stability problems caused by carrier and power frequency harmonics.

The preamplifier is constructed on two printed circuit boards. The first board (labelled Preamp #1) contains A8, A9, and their associated circuitry, and the second board contains the other two amplifiers and

components. The division between the two boards is indicated in Fig. A-4 by a dotted line.

The preamplifier requires ± 15 volts at 60 milliamps. The 10 μF capacitors bypassing the power supply connections to A8 are necessary because of the high gain-bandwidth product of this stage.

2.2.4 Null Signal Amplifier and Phase Shifter

The high temperature environment for which the skin-friction sensor was designed dictated construction techniques which make alignment to close tolerances very difficult. Therefore an electrical null was added to the control system. To achieve this null signal, the carrier signal across the armature is sensed. It is then amplified and filtered by A2, A3, and their associated components. R31 adjusts the amplitude, and the remainder of the circuit is a unity gain phase shifter. The phase of the null signal can be adjusted from 0° to 180° by R36.

The whole circuit is built on one printed circuit board and requires ± 15 volts at 30 milliamps.

2.2.5 Ring Demodulator and Compensating Amplifier

The ring demodulator is a full-wave discriminator which produces a polarized d-c voltage corresponding to the phase relationship of the signal from the preamplifier with respect to the reference signal and to the amplitude of the input signal. For proper operation the reference signal should be greater than twice the maximum amplitude of the input signal. In this case the reference signal is adjusted to eight volts rms where the maximum input signal is one volt rms.

Variable resistors R84 and R85 are adjusted for zero d-c output with no input and a balanced full-wave output. The low pass filter composed of R88 and C40 attenuate carrier frequency harmonics.

The compensating amplifier is on the same printed circuit board as the demodulator. It consists of amplifier A12 and associated components.

The compensating amplifier provides the necessary d-c gain to achieve the desired overall loop gain constant of 90 and the lag and lead networks

needed for closed-loop stability at this gain and desired bandwidth of 20 Hz. The transfer function of the compensation is

$$\frac{E_o(s)}{E_i(s)} = \frac{2.3(1 + 0.176s)(1 + 0.0156s)}{(1 + 2.33s)(1 + 2.71 \times 10^{-3}s)}$$

The compensating amplifier requires ± 15 volts at 10 milliamps.

2.2.6 Reference Amplifer and Phase Shifter

The reference signal for the demodulator is provided by the carrier generator, phase shifter, and reference amplifier. The phase shifter is identical to the null signal phase shifter. The phase shift is adjusted by potentiometer R93. The reference amplifier provides filtering with a double pole at 5 KHz and has a gain of 40 at 5 KHz to provide the eight volts rms reference for the demodulator.

The reference amplifier and phase shifter requires ± 15 volts at 10 milliamps.

2.2.7 Limiter

The limiter is inserted in the control loop between the compensation amplifier and the power amplifier to prevent saturation of the power amplifier, especially during turn-on. The limiter limits both positive and negative swings to 0.93 volts, and the positive and negative limits are set by R108 and R107 respectively. Between the two limits the limiter has a linear gain of approximately 1.5.

The output of the limiter is the error signal that is fed back to the power amplifier and superimposed on the carrier.

The limiter requires ± 15 volts at 10 milliamps.

2.2.8 Field Constant Current Sources

The torque constant of the motor is proportional to the armature current for a constant flux in the field coils, but the converse is also true. Therefore, because this system employs armature control, the flux (i.e., the current) of the field coils must be held constant. This is

particularly important in this application because the resistance of the field coils increases by a factor of six as the temperature is increased to 2000°F (1093°C).

The constant flux requirement is met by driving the field coils with separate constant current sources, with d-c loop gains of 100. This reduces the error in force readout due to heating of the field coils to an experimentally measured value of 1.1%.

An additional requirement of the current sources is low attenuation of the carrier induced sensor signal by the 10 ohm resistors across Q14 and Q17. This requirement is met by keeping the loop gain high at the carrier frequency with a value of 50 at 5 KHz.

The field current sources require ± 30 volts at 5 amps and ± 15 volts at 40 milliamps. The field current sources and coils are protected by 5 amp fuses in series with the coils.

3.0 CONTROL CIRCUIT ALIGNMENT PROCEDURE

This section contains a detailed alignment procedure for the electronic control circuit. This alignment procedure must be followed whenever any component of the skin-friction meter is changed, especially if the change results in phase shifts between the carrier and null signals. The locations of the adjustments and test points are shown in Fig . A-5.

Note: All adjustments in this section are made with the control loop open. Disconnect the cable from the input to the power amplifier labelled "INPUT FROM LIMITER". Terminate the cable with a 4.7 kΩ resistor and short the input connector.

3.1 Gain and Carrier Generator Level Adjustment

With no power applied to the control system, the carrier generator output is adjusted to 620 millivolts peak to peak at a frequency of 5 KHz. At this carrier generator amplitude, the system gain, R1, is adjusted until 570 millivolts appears on the wiper of R1.

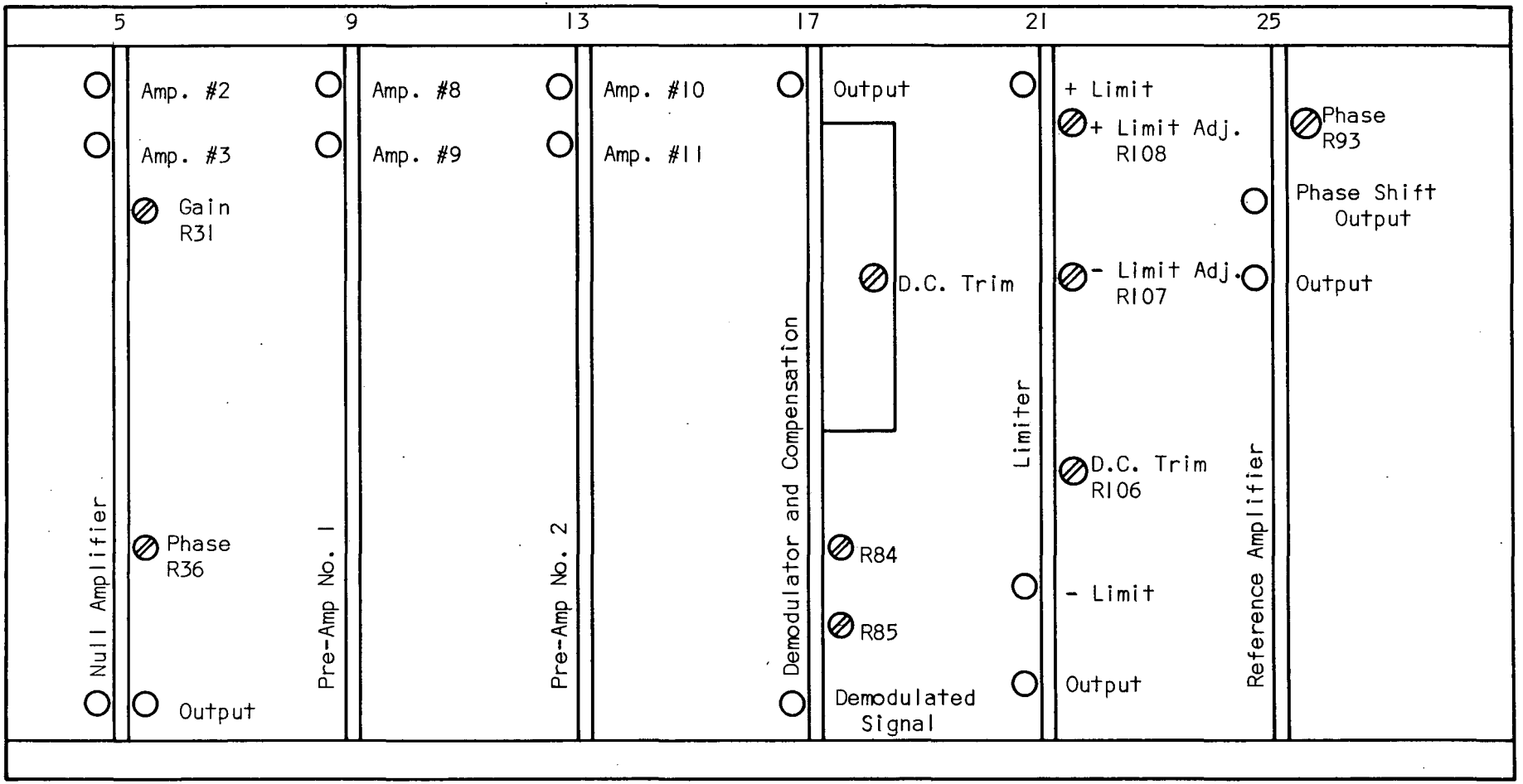

Figure A-5 Signal Conditioning Chassis Adjustment and Test Point Location

3.2 Field Current Source and Field Signal Adjustment

Turn on SW1, the ± 15 volt power supply, and the ± 30 volt power supplies to the field current sources in that order. Both meters on the field current source chassis should read 3.5 amps after approximately 1 minute. The current adjustments are R38 and R51 for field 1 and field 2, respectively.

3.3 Null Signal and Reference Phase Adjustment

With the field signal leads connected, connect an oscilloscope to the output of preamp 1. Adjust the phase of the null amplifier, R36, for minimum amplitude. Then adjust the gain of the null amplifier, R31, for minimum amplitude. Repeat these adjustments until no further amplitude reduction can be obtained. After the initial adjustment the oscilloscope can be changed to the output of preamp 2 for increased sensitivity.

Compare the phase of the outputs of preamp 2 and the reference amplifier. Adjust the phase of the reference amplifier for 180° phase difference.

3.4 Null Adjustment

With an oscilloscope connected to the output of the limiter and the motor armature centered (free), fine adjust the gain of the null signal amplifier, R31, until the output of the limiter is zeroed. Lightly blowing on the armature should now produce a voltage that oscillates about zero with little damping.

3.5 Control Loop Gain

The control loop gain should be checked after the above procedure has been completed. This measurement is made by recording the voltage from the limiter (terminated in 4.7 kΩ) produced by a 200 millivolt step applied to the power amplifier input labelled "INPUT FROM LIMITER" which had been shorted during all preceeding adjustments. This measurement is most easily made with a two channel chart recorder.

If the gain of the system is correct, the loop gain should be 90 volts/volt. If the gain is low, the alignment should be repeated.

If the above procedure has been successfully completed, the loop can now be closed. The 4.7 kΩ termination on the output of the limiter and the short on the input to the power amplifier are removed, and the cable is connected to complete the loop. This should be done with the system turned off.

4.0 FURTHER ADJUSTMENTS

The preceeding section described the adjustments that have to be performed to obtain the correct loop gain and alignment. The adjustments described in this section should not ordinarily have to be performed unless some component in the specific circuit is changed.

4.1 Power Amplifier Zero and Distortion Adjustment

Both inputs to the power amplifier should be shorted, and the output should be loaded (either the armature coil or 4 Ω resistor).

With the ± 15 volt and ± 30 volt power supplies turned on, the output current should be zero. If the output current is not zero, R9 should be adjusted. After the amplifier has been zeroed, the no-signal current from each power supply should be approximately 150 ma. The quiescent drain is adjusted by the distortion adjust, R19.

APPENDIX B

FINAL TESTS

Final tests were made on the skin friction meter during July 1971. Tests were performed in a temperature controlled oven using a pendulum as a method of applying force to the sensor. A schematic of this arrangement is shown in Fig. B-1.

The pendulum length was 30 inches and the pendulum weight was .22 lbs. This gave a force on the sensor of 7×10^{-6} lb/mil of micrometer movement. This force range was too low to test the sensor over its complete range. This fault resulted from having to modify the original design to give proper clearance around the armature counterweight.

Figure B-2 gives results of the force testing for increasing and decreasing forces at 90°F and for increasing forces at 400°F. Linearity is very good. The small deadband at zero output represents clearance between the pendulum knife edges and the string. The full scale output of the sensor is 100 mw.

Numerous runs were made at increasing oven temperatures, and copies of the strip chart recordings have been forwarded to the contract monitor.

The system became unstable at 600°F with a large applied force. After several attempts to stabilize it by changing the control inputs, the oven was turned off. Stability was regained at 520°F.

The stability problem was re-examined by heating to 550°F without force application. The system became unstable. The temperature was increased to 600°F and a measure of stability was obtained but the system was unstable again at 650°F. At 750°F the system was stable but very noisy. Individual force steps could be distinguished but the range was somewhat limited. The oven was turned off and smooth force applications were made at intermediate temperatures, but the system became unstable again at less than 600°F.

This cause of the instability is not known at this time. Several factors in the test set-up probably have a strong effect. One is that

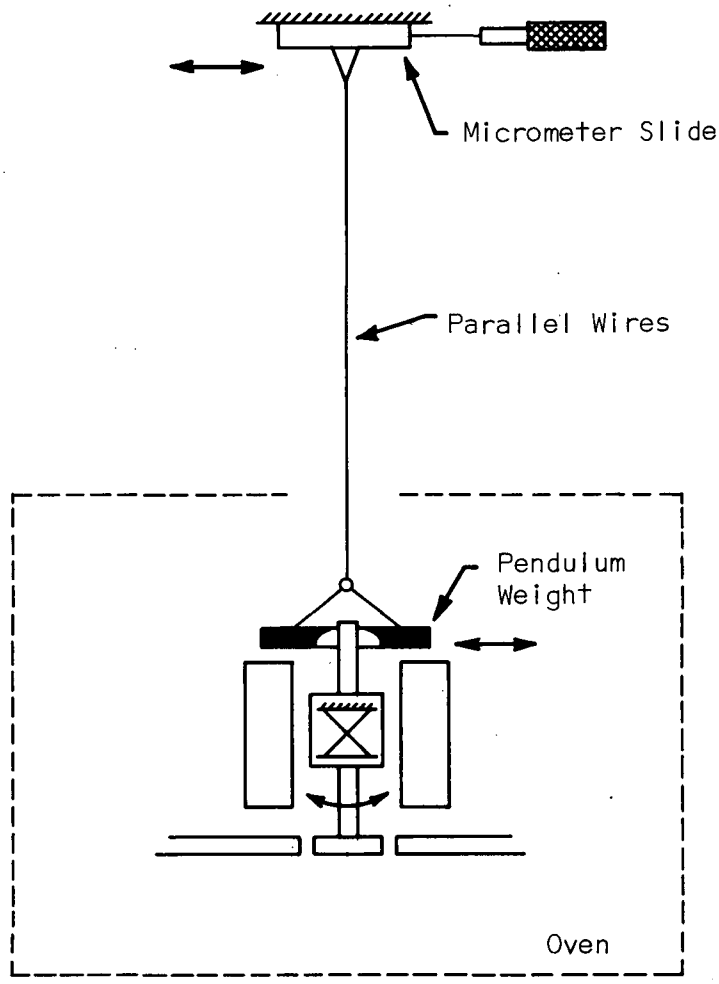

Figure B-1

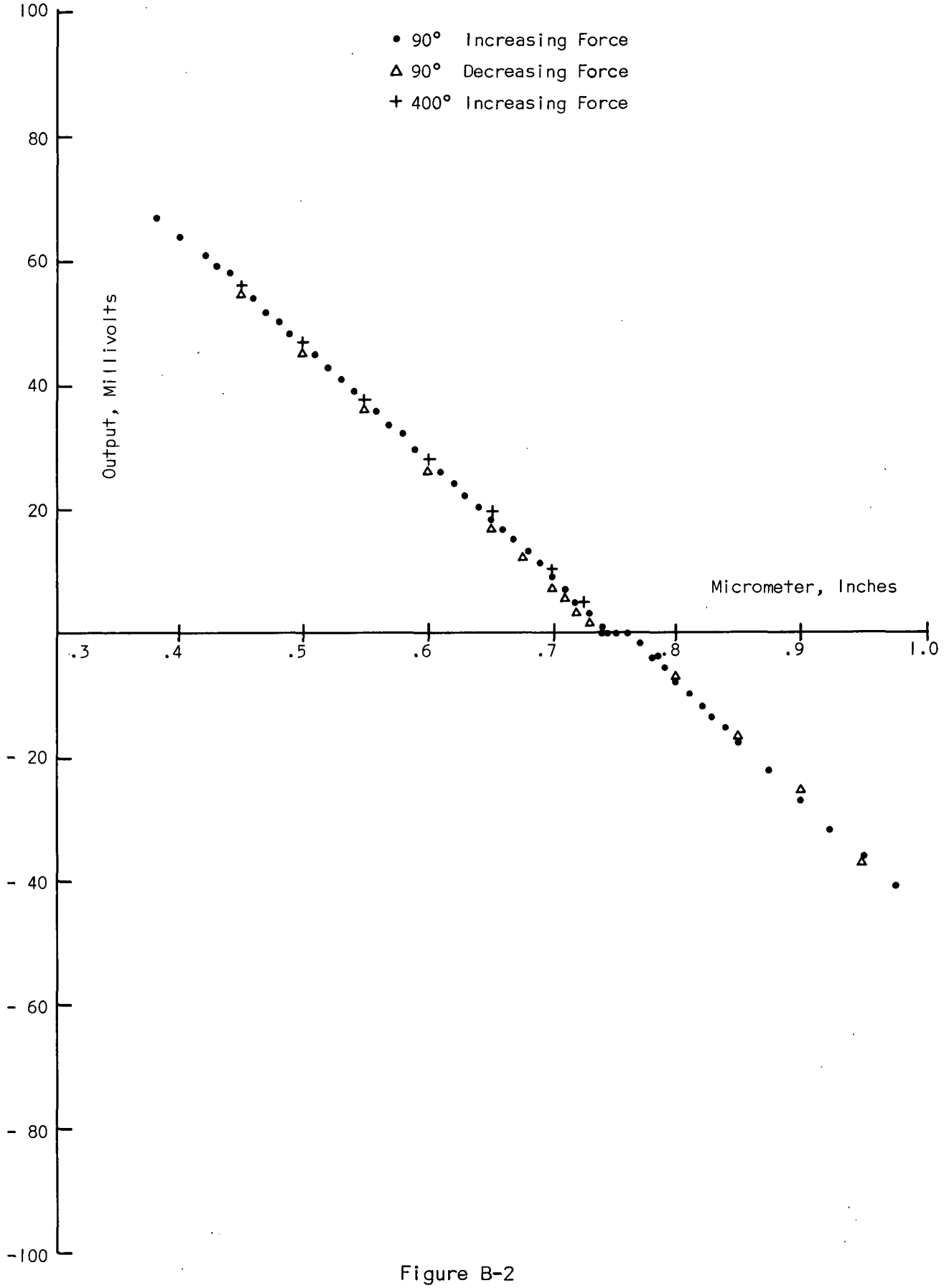
• 90° Increasing Force
Δ 90° Decreasing Force
+ 400° Increasing Force
Output, Millivolts
Micrometer, Inches
100
80
60
40
20
- 20
- 40
- 60
- 80
-100
.3
.4
.5
.6
.7
.8
.9
1.0

Figure B-2

the mass of the pendulum enters into the dynamics of the armature and changes the natural frequencies of the total system away from those for which the system was compensated. The other factor is that the system endures long soak times on the order of several hours at high temperatures. This is different from what will be encountered in wind tunnel use where the run times are on the order of a minute or less. It is hoped that wind tunnel testing will shed new light on this problem.